Uncertainty in modeled Arctic sea ice volume

Axel Schweiger,[1] Ron Lindsay,[1] Jinlun Zhang,[1] Mike Steele,[1] Harry Stern,[1] and Ron Kwok[2]

Received 25 February 2011; revised 27 April 2011; accepted 7 June 2011; published 27 September 2011.

[1] Uncertainty in the Pan-Arctic Ice-Ocean Modeling and Assimilation System (PIOMAS) Arctic sea ice volume record is characterized. A range of observations and approaches, including in situ ice thickness measurements, ICESat retrieved ice thickness, and model sensitivity studies, yields a conservative estimate for October Arctic ice volume uncertainty of 1.35×10^3 km^3 and an uncertainty of the ice volume trend over the 1979–2010 period of 1.0×10^3 km^3 decade^{-1}. A conservative estimate of the trend over this period is -2.8×10^3 km^3 decade^{-1}. PIOMAS ice thickness estimates agree well with ICESat ice thickness retrievals (<0.1 m mean difference) for the area for which submarine data are available, while difference outside this area are larger. PIOMAS spatial thickness patterns agree well with ICESat thickness estimates with pattern correlations of above 0.8. PIOMAS appears to overestimate thin ice thickness and underestimate thick ice, yielding a smaller downward trend than apparent in reconstructions from observations. PIOMAS ice volume uncertainties and trends are examined in the context of climate change attribution and the declaration of record minima. The distribution of 32 year trends in a preindustrial coupled model simulation shows no trends comparable to those seen in the PIOMAS retrospective, even when the trend uncertainty is accounted for. Attempts to label September minima as new record lows are sensitive to modeling error. However, the September 2010 ice volume anomaly did in fact exceed the previous 2007 minimum by a large enough margin to establish a statistically significant new record.

Citation: Schweiger, A., R. Lindsay, J. Zhang, M. Steele, H. Stern, and R. Kwok (2011), Uncertainty in modeled Arctic sea ice volume, *J. Geophys. Res.*, *116*, C00D06, doi:10.1029/2011JC007084.

1. Introduction

[2] Arctic sea ice volume is an important indicator of global climate change. Unlike sea ice extent, sea ice volume is more directly related to the energy balance, because a loss or gain in sea ice volume represents a specific change in latent heat. Changes in Arctic sea ice volume thus provide a gauge of our understanding of global climate, and predictive global climate models should be able to reproduce observed changes in sea ice volume. Moreover, global climate model simulations with increasing anthropogenic greenhouse gas forcing show that the decline in Arctic sea ice volume will outpace the decline in sea ice extent on a percentage basis from 1990 to the end of the 21st century by as much as a factor of two [*Gregory et al.*, 2002; *Intergovernmental Panel on Climate Change*, 2007], thus making ice volume a more sensitive climate indicator than ice extent. The greater sensitivity of ice volume is in part due to the geographical controls of winter sea ice extent in the Northern Hemisphere which minimize interannual changes in winter ice extent [*Eisenman*, 2010].

[3] Sea ice extent has been well measured from space for the past 30 years using passive microwave instruments. Unfortunately a long-term record of sea ice volume is much more difficult to establish, since it depends on reliable information about ice thickness in addition to ice extent. In situ measurements of thickness are spotty in time and space, yielding a poor sampling of the spatial and temporal variability. Satellite-based retrievals of ice thickness using RADAR or LIDAR altimeters [*Giles et al.*, 2008; *Kwok et al.*, 2009] have recently become available but their record is still relatively short and the retrieval techniques are subject to a variety of errors. Sea ice volume can also be estimated from the age of sea ice, which can be derived from buoy or satellite-derived ice motion and ice extent maps in combination with empirical relationships between age and thickness [*Maslanik et al.*, 2007].

[4] Another approach to estimating the total ice volume over an extended period of time is to use a coupled ice-ocean model which simulates variations of ice thickness and extent by modeling the thermodynamic and dynamic processes that influence sea ice variations [*Zhang et al.*, 2010]. In order to improve simulations, the model solution can be constrained through the assimilation of observed

[1]Polar Science Center, Applied Physics Laboratory, University of Washington, Seattle, Washington, USA.
[2]Jet Propulsion Laboratory, California Institute of Technology, Pasadena, California, USA.

Copyright 2011 by the American Geophysical Union.
0148-0227/11/2011JC007084

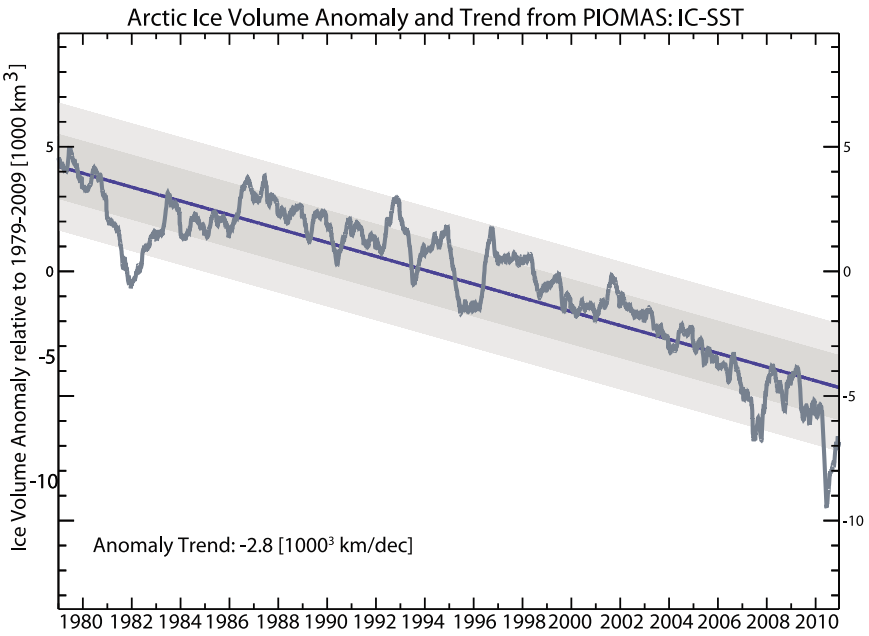

Figure 1. Daily Arctic sea ice volume anomaly from PIOMAS. The daily anomaly is computed relative to the average for the day of the year computed over the 1979–2009 period. The trend is computed from 1979 to 2010. Shaded areas show the standard deviations (× 1 and × 2) of the residuals of the trend. Updated versions are available at http://psc.apl.washington.edu/wordpress/research/projects/arctic-sea-ice-volume-anomaly/.

information such as ice concentrations or sea surface temperature. The Pan-Arctic Ice-Ocean Modeling and Assimilation System (PIOMAS) developed at the Polar Science Center (PSC), University of Washington is such a system. An example of sea ice volume estimates from PIOMAS is shown in Figure 1. Although PIOMAS ice thickness has previously been validated against ice thickness measurements from U.S. submarines at a limited number of times and locations [*Zhang and Rothrock*, 2003], a systematic assessment of uncertainties in ice volume and trends is still needed. This paper attempts to fill this gap.

[5] This paper is organized as follows: We first introduce the model and various data sources used to establish uncertainty estimates (section 2). Since ice volume estimates are difficult to validate directly, we examine how well PIOMAS ice thickness estimates match in situ and satellite observations (section 3). Trends in ice thickness and their uncertainty are examined in section 4. We then assess how the uncertainty estimates for ice thickness affect the uncertainty of the total ice volume and volume trends (section 5). Ice volume anomalies and uncertainty estimates are then put into the context of applications (section 6), i.e., how uncertainty affects the attribution of trends and the detection of record minima. Given sampling issues and uncertainties in the validation data, we employ a range of approaches and data sets to find bounds of the uncertainty. Results for the uncertainty estimates are summarized in Tables 1–4.

2. Model and Data

2.1. PIOMAS

[6] The coupled ice-ocean model used to derive Arctic sea ice volume is the Pan-Arctic Ice-Ocean Modeling and Assimilation System. It consists of a multicategory thickness and enthalpy distribution sea ice model [*Zhang and Rothrock*, 2003] coupled with the Parallel Ocean Program developed at the Los Alamos National Laboratory. The sea ice model employs a teardrop viscous plastic rheology [*Zhang and Rothrock*, 2005], a mechanical redistribution function for ice ridging [*Hibler*, 1980; *Thorndike et al.*, 1975], and a LSR (line successive relaxation) dynamics solver [*Zhang and Hibler*, 1997]. The model covers the region north of 48°N and is one way nested to a similar but global ice-ocean model [*Zhang and Rothrock*, 2005]. PIOMAS is capable of assimilating satellite ice concentration data following [*Lindsay and Zhang*, 2006]. It is also capable of assimilating observations of sea surface temperature (SST) following *Manda et al.* [2005]. Daily mean NCEP/NCAR reanalysis data are used as atmospheric forcing, i.e., 10 m surface winds, 2 m surface air temperature (SAT), specific humidity, precipitation, evaporation, downwelling longwave radiation, sea level pressure, and cloud fraction. Cloud fraction is used to calculate downwelling shortwave radiation following *Parkinson and Washington* [1979].

[7] Three different PIOMAS integrations are discussed in this paper. The first is an integration that assimilates ice concentration only (IC). Ice concentrations are from the Hadley Centre for 1958–1995 and from NSIDC for 1996 to present. Another integration (IC-SST), in addition to ice concentrations, assimilates sea surface temperature (SST) from the NCEP/NCAR reanalysis based on the global daily high-resolution Reynolds SST analyses using satellite and in situ observations [*Kalnay et al.*, 1996; *Reynolds and Marsico*, 1993; *Reynolds et al.*, 2007]. A third integration (model only) assimilates no data. For the model-only and IC-SST cases, the parameterization of ice strength is based on *Hibler*

Table 1. Mean Ice Thickness (m) Random Uncertainty and Mean Error Estimates Determined Using Different Data Sets[a]

	Sea Ice CDR			ICESat	
	RMSD	r	Mean	RMSD	Mean
DRA	0.76	0.73	−0.17	Spring: 0.4, Fall: 0.3	Spring: 0.1, Fall: 0.0
ICESat domain	**0.78**	0.73	−0.01	Spring: 0.19, Fall: 0.29	Spring: −0.1, Fall: **−0.26**

[a]Regional mean biases for two different areas are provided. Conservative estimates (bold) of the random error and the mean error are the largest absolute estimates.

[1979], while the parameterization of ice strength for the IC case is based on *Rothrock* [1975] and *Hibler* [1980]. The choice of these integrations reflects the evolution of model development and tuning which typically involves multiple integrations. These three integrations represent the latest state of the PIOMAS model development and have shown good validation statistics for ice thickness (greater than 50% explained variance) when compared with submarine-based upward looking sonar (ULS) measurements. The choice of these runs is not meant to provide a comprehensive assessment of the relative benefits of assimilating different data sets as done by *Lindsay and Zhang* [2006]. As we will show later, the IC-SST run provides the most conservative assessment of the long-term trend and is therefore used as the reference integration throughout the paper.

2.2. In Situ Measurements From the Sea Ice Thickness Climate Data Record

[8] A sea ice thickness climate data record (sea ice CDR) of in situ observations of ice draft and thickness has recently been created [*Lindsay*, 2010]. This record integrates sea ice draft measurements from submarine upward looking sonar, moored ULS, and airborne electromagnetic (EM) measurements from a variety of sources into a single place and format. The sources include U.S. submarines [*Tucker et al.*, 2001; *Wensnahan and Rothrock*, 2005] moored ULS from the eastern Beaufort Sea [*Melling and Riedel*, 2008], the central Beaufort Gyre (Beaufort Gyre Exploration Project based at the Woods Hole Oceanographic Institution, http://www.whoi.edu/beaufortgyre), Fram Strait [*Witte and Fahrbach*, 2005]; airborne EM-based thickness measurements [*Haas et al.*, 2009, 2010], and ULS measurements at the North Pole Environmental Observatory (NPEO).

[9] Submarine-based ULS and airborne EM measurements are provided as 50 km averaged segments. Following *Rothrock et al.* [2008, hereinafter RPW08], all draft observations from submarines and moorings are converted to ice thickness using an ice density of 928 kg m^{-3} and the snow water equivalent estimated by the model. Uncertainty in the draft-to-thickness conversion is relatively small (<10% of draft). EM measurements provide the combined thickness of ice thickness plus the overlying snow cover [*Haas et al.*, 2010]. They are converted to thickness using the snow depth estimated from the snow water equivalent accumulated during the PIOMAS integrations assuming a seasonal variation in snow density [RPW08]. ULS measurements provide a first return measurement which can lead to a bias in ice draft [*Vinje et al.*, 1998]. This bias depends on the field of view of the ULS instrument, its deployment depth, and the thickness distribution itself. *Rothrock and Wensnahan* [2007] estimate a bias of 0.29 m for the submarine record they investigated. Following *Kwok and Rothrock* [2009, hereinafter KR09], we subtract this bias from submarine draft measurements prior to the comparison with model observations. No bias corrections were applied to measurements other than the U.S. submarine ULS data, because such bias corrections are not readily available and the development of such bias corrections is beyond the scope of this study. Similarly, following RPM08, measurements from the U.K. submarine were not used in this analysis since their processing history is uncertain.

[10] Each sea ice CDR observation was then paired with a monthly mean model thickness using the closest model grid cell. For in situ measurements from moving platforms (submarines and airborne EM) the in situ measurement does not really correspond to a monthly average (the submarine may cross the entire Arctic in a few days) so that this pairing does include a temporal sampling error.

2.3. ICESat

[11] Ice thickness estimates from the Geophysical Laser Altimetry System (GLAS) on ICESat have recently become available [*Kwok and Cunningham*, 2008; *Zwally et al.*, 2008]. The ICESat retrieval algorithm measures ice freeboard by comparing the satellite distance from the snow or ice surface to that of ice-free areas. Freeboard measurements are then converted to ice thickness using a sequence of processing steps, accounting for snow loading, atmospheric pressure, and sampling biases [*Kwok et al.*, 2009, hereinafter K09]. Given that ice freeboard amounts to only about 10%

Table 2. Ice Thickness Trends (m $decade^{-1}$) Determined Using Different Methodologies[a]

	PIOMAS 1979–2010			
	Mar	Oct	Paired 10 Year+ Trends[b]	KR09 1979–2007
DRA	IC-SST: **−0.25**, IC: −0.37, Model only: −0.36	IC-SST: **−0.39**, IC: −0.47, Model only: −0.53	Observed: −0.48, IC-SST: −0.42	Mar: −0.53, Oct: −0.50
PIOMAS domain[c]	IC-SST: **−0.15**, IC: −0.19, Model only: −0.20	IC-SST: **−0.25**, IC: −0.33, Model only: −0.37		

[a]Conservative estimates (bold) are the smallest downward trend estimate for each domain and season.
[b]Some observations are from outside the DRA.
[c]Thickness trends for the PIOMAS domain were computed using a minimum thickness threshold of 0.15 m to exclude the extensive areas of open water.

Table 3. Total Sea Ice Volume (10^3 km^3) Random Uncertainty and Mean Error Estimates Determined Using Different Methodologies[a]

	Sea Ice CDR	PIOMAS Adjusted to CDR	Three Model Runs	ICESat
Random uncertainty	Mar: 0.1, Oct: 0.07	0.76	Mar: **2.25**, Oct: **1.35**	
Biases	Mar: **−2.8**, Oct: −1.5			Spring: −1.7, Fall: **−2.3**

[a]Conservative estimates (bold) are the largest absolute estimates for each season.

of the total thickness, space-based thickness retrievals are highly sensitive to potential errors associated with these steps. K09 estimates ICESat thickness uncertainties to be 0.5 m for individual 25 km ICESat grid cells. Fields of mean ice thickness are available at the following URL (http://rkwok.jpl.nasa.gov/icesat/). These ice thickness fields are composites generated from ten ICESat campaigns during October–November 2003–2007 and March–February 2004–2008. Because of the small footprint nadir sampling of the ICESat instrument, these fields are composites of sea ice thickness from a range of times during the observation intervals and treating them as averages incurs a sampling error.

[12] For direct comparison with PIOMAS, PIOMAS ice thicknesses were regridded to the ICESat grid using nearest neighbor interpolation. Monthly PIOMAS averages for March were used for comparison with the ICESat spring campaigns, and combined October and November averages were used for comparisons with the ICESat fall campaigns. The averages are thought to best correspond to the temporal sampling of ICESat composites. To address the nature of the ICESat retrieval, which does not fully account for varying ice concentrations but assigns the retrieved thickness to the entire grid cell, an additional weighting using AMSR-derived ice concentrations is needed. Following KR09, AMSR-derived ice concentrations at 25 km resolution were obtained from NSIDC and concentration-weighted ICESat thickness for each grid cell was calculated by multiplying the ICESat ice thickness with the AMSR-derived ice concentration.

[13] The calculation of ICESat thickness averages includes observations where the ice thickness is 0. This distinction is consistent with the usage by K09 and KR09 and corresponds to the definition of effective ice thickness often used in sea ice modeling:

$$h_{eff} = \sum g(h_i)h_i, \quad (1)$$

where *g(h)* is the discrete thickness distribution or fraction of grid cell covered by ice thickness h_i, including $g(h = 0)$. It does however mean that the mean ice thickness for a given area is strongly influenced by variations in ice concentrations but that ice volume can simply be estimated from h_{eff} and the area of the grid cell. Whether or not the open water thickness category is included in the definition of mean ice thickness is not always clear in the pertinent literature, so it is specifically stated here.

2.4. Time Series of Regional Mean Ice Thickness

[14] KR09 recently published an assessment of ice thickness changes from U.S. submarine data for a part of the Arctic Ocean for which U.S. submarine data have been released (the data release area (DRA)). In this assessment, the inhomogenous temporal and spatial sampling of the submarine-based draft measurements was addressed by fitting polynomials to U.S. submarine draft observations that express ice thickness as a function of space, seasonal cycle and time [RPW08]. These polynomials are then evaluated for the DRA and concatenated with ICESat ice thickness estimates for the DRA. KR09 estimate the standard deviation of the total uncertainty of the regression model-derived thickness for the DRA to as 0.5 m. The corresponding ICESat uncertainty is estimated as 0.37 m. We use this time series for comparison with PIOMAS-derived ice thickness time series.

2.5. Community Climate System Model Version 3 Runs

[15] IPCC integrations for (1) the preindustrial control, (2) the climate of the 20th century (20C3M), and (3) the A1b scenario run for the NCAR Community Climate System Model Version 3 (CCSM3) model were obtained from the World Climate Research Programme's (WCRP's) Coupled Model Intercomparison Project Phase 3 (CMIP3) multimodel data set archive [*Meehl et al.*, 2007]. Sea ice concentration and thickness were retrieved and total ice volume, ice area, and ice extent calculated. Anomalies were calculated relative to the 1958–1978 period and expressed as percentage of means. Additional IPCC AR4 runs for the subset of models identified as having a better representation of sea ice variability [*Wang and Overland*, 2009] were also extracted and processed in the same way (Table 5).

3. Ice Thickness Uncertainties

3.1. Local Uncertainties From In Situ Observations From the Sea Ice CDR

[16] Measurements of total arctic ice volume do not exist, therefore validation of modeled ice volume must rely on local measurements of ice thickness. We here analyze separately ice thickness observations that were or were not used during PIOMAS model development. Figures 2 and 3 show comparisons of PIOMAS draft estimates with sea ice CDR draft observations for submarine and all other measurements, respectively. The correlations for the data which were or were not used in model development are identical (0.73) and RMS differences are very close (0.76 versus 0.78 m). Mean errors are actually slightly better (–0.17 versus –0.01 m) when excluding submarine measurements. The mean thickness is over a meter smaller for the non U.S.

Table 4. Sea Ice Volume Trends (1979–2010, 10^3 km^3 decade^{-1}) and Uncertainty Estimates Determined Using Different Methodologies[a]

	Sea Ice CDR	PIOMAS Adjusted to CDR	Three Model Runs
Trend		−3.5	**−2.8** to −3.8
Uncertainty	0.07	−0.7	**1.0**

[a]Conservative estimates (bold) are the smallest downward trend and the largest uncertainty estimate.

Table 5. Model Abbreviation and Source Institutions for the Subset of PCMDI Archived AR-4 Models Used in This Study

Model Abbreviation	Institutions	Subgrid-Scale Ice Thickness Distribution
CCSM3	National Center for Atmospheric Research, USA	Yes
MIROC (medium-resolution)	Center for Climate System Research (University of Tokyo), National Institute for Environmental Studies, and Frontier Research Center for Global Change, Japan	No
IPSL	Institute Pierre Simon Laplace, France	No
ECHO-G	Meteorological Institute of the University of Bonn and the Meteorological Research Institute of KMA, Model and Data Group, Germany	No
GEM-1	Hadley Centre for Climate Prediction and Research, Met Office, UK	Yes
CNRM	Météo-France, Centre National de Recherches Météorologiques, France	Yes

submarine data because most of the other data are from a later period, reflecting the thinning of the ice cover. Using these local thickness uncertainties as a measure of model uncertainty, we can compute uncertainties in volume and trends. This is done in section 5.1.

[17] What do the high correlations between PIOMAS and in situ observations tell us? Are they simply the result of the ability of the model to capture the strong annual cycle of growth and melt and say little about the model's ability to capture the long-term trend? To examine the effect of the annual cycle on the validation statistics, we compare the PIOMAS model results with in situ observations from the sea ice CDR for the ICESAT observation periods February–March and October–November separately. These times are close to the maximum and minimum of the annual ice thickness cycle and provide a sufficiently large number of observations to allow a meaningful comparison. Performance of PIOMAS with respect to observations for spring (February–March) is excellent, with a correlation of 0.83 and a mean bias of −0.08 m. RMS differences for February–March are 0.61 m. Comparisons for fall (October–November) are somewhat worse with a correlation of 0.65, an RMS error of 0.76 m, and a bias of –0.03 m. In general, relative to the sea ice CDR observations, the model tends to overestimate the thickness of thinner ice and underestimate the thickness of thick ice. These results demonstrate that the model captures ice thickness variability beyond the annual cycle, suggesting that long-term spatial and temporal variability may be well represented. We will revisit each of those separately below.

[18] Note that observations from the North Pole Environmental Observatory (NPEO) were excluded from the above analysis. A comparison of NPEO data with PIOMAS shows that some of the earlier NPEO ULS measurements

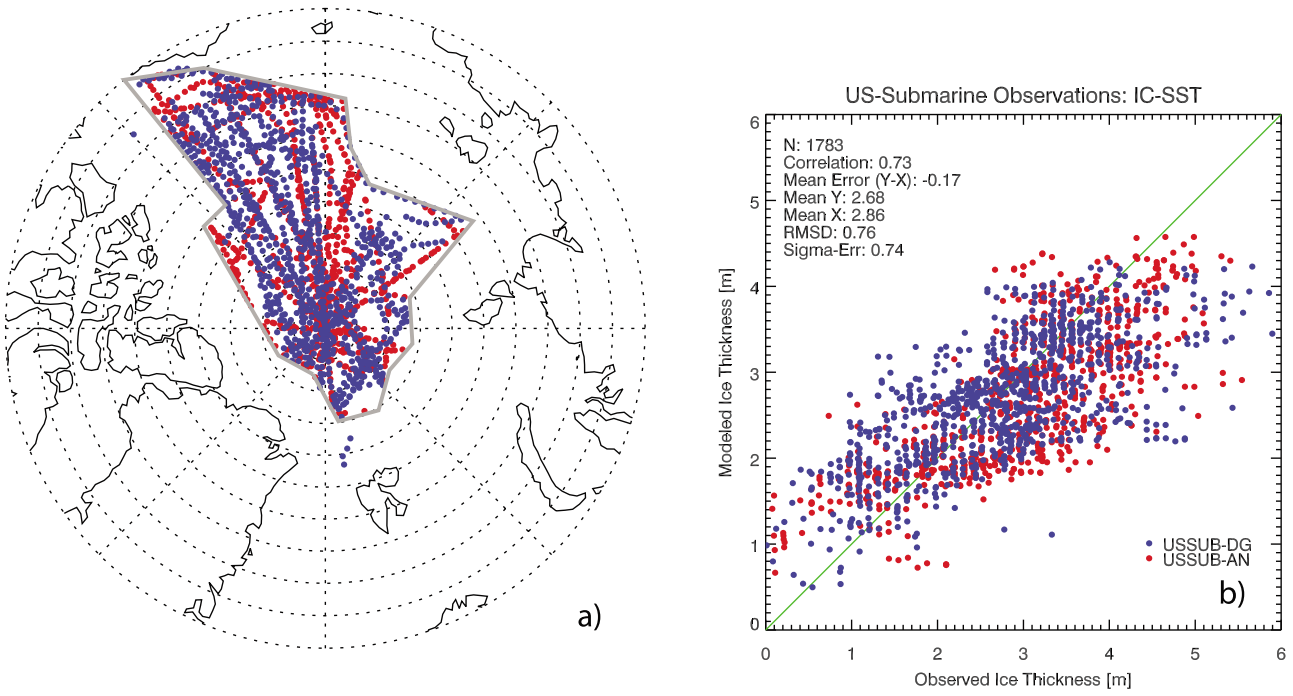

Figure 2. Comparison of PIOMAS ice thickness estimates with observations from U.S. submarines. The DRA is shown in gray in Figure 2a. USSUB-DG and USSUB-AN labels refer to U.S. submarine digital and analog recordings, respectively. The data covers the period 1975–2005.

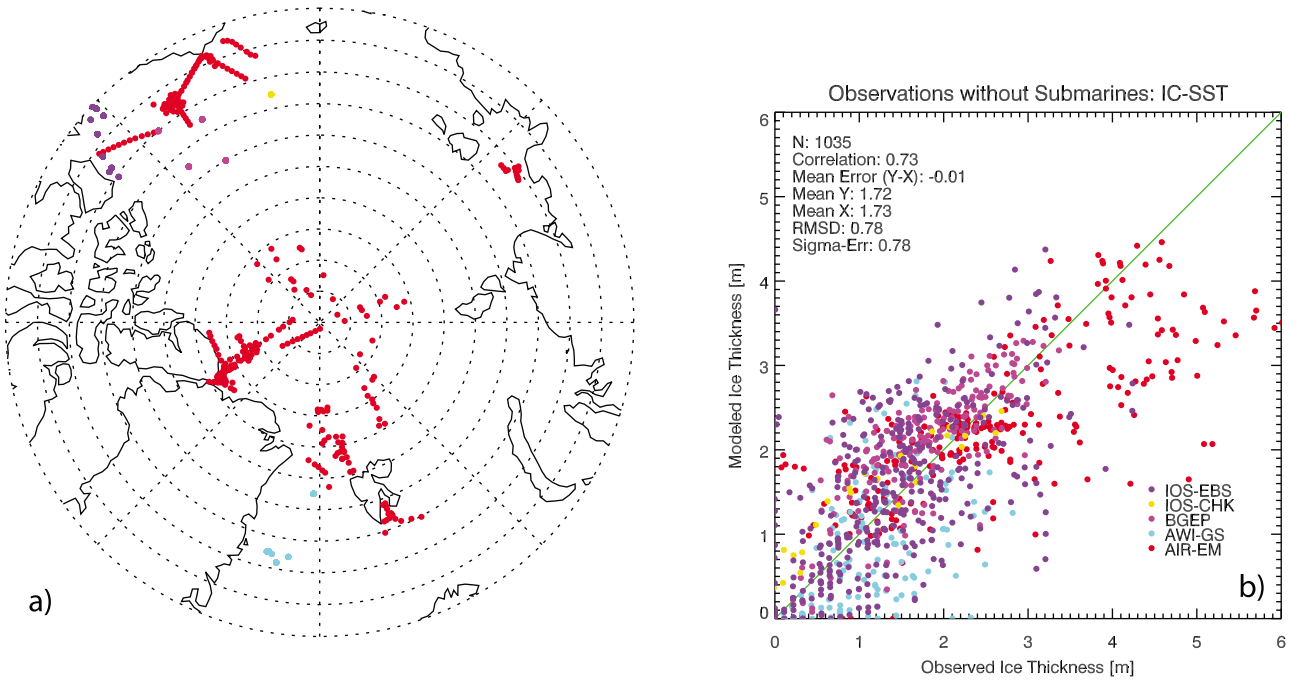

Figure 3. Comparison of PIOMAS ice thickness estimates with observations excluding the U.S. submarine observations. (a) Location map of ice thickness observations used for this comparison. (b) Comparison of observations with PIOMAS (IC-SST). Colors indicate different data sources for ice thickness measurements. Institute of Ocean Sciences-Eastern Beaufort Sea (IOS-EBS) and -Chukchi Sea (IOS-CHK), Woods Hole Oceanographic Institution-Beaufort Gyre Exploration Projects (BGEP), Alfred Wegener Institute-Greenland Sea (AWI-GS), and Alfred Wegener Institute and University of Alberta Airborne-Electromagnetic Induction (AIR-EM).

have much thicker ice than previous observations at this location, and seem to be inconsistent with recent measurements of ice thickness from EM data near the North Pole which have near 0 bias and correlations of 0.93 relative to the model (Figure 4). NPEO ULS data from instruments deployed in 2006 and 2008 show a much better agreement with PIOMAS and EM observations. Though no direct overlap between the earlier NPEO data and EM data exists, it is difficult to imagine why the model would perform well with little bias in the area near the North Pole except for 2001–2005 when differences with NPEO are large. At this point we do not have a solid explanation for this discrepancy between the pre-2006 NPEO data and the model. A more detailed investigation is underway (D. Moritz, personal communication, 2011).

3.2. Uncertainties in Regional Mean Ice Thickness (Biases)

[19] Random errors established from individual in situ observations affect regional mean ice volume estimates proportional to $N^{-1/2}$, (N is the number of grid cells in model or retrieval). Since N may be large (depending on the size of the region), ice volume uncertainty estimates are dominated by biases rather than random errors [KR09] (also discussion in section 5.1). We use ICESat-derived regional means for both the DRA and the ICESsat domain to assess potential biases in PIOMAS regional mean ice thickness.

[20] Figure 5a shows a comparison of ice thickness for the ICESat domain (see Figure 6) from PIOMAS (IC-SST) and ICESat. ICESat thickness estimates exceed PIOMAS estimates by 0.1 and 0.26 m for February–March and October–November, respectively, well within the uncertainty of ICESat estimates of 0.37 m [KR09]. While the difference between PIOMAS and ICESsat in February–March (−0.1 m) is of the same order as that between the model and in situ observations in the sea ice CDR, October–November model-ICESat differences are substantially higher (−0.26 m) relative to model–in situ observation differences. Reasons for this discrepancy will become apparent when we compare spatial patterns (section 3.3). Model-ICESat differences are smaller over the DRA domain (Figure 5b), possibly reflecting the use of submarine draft data over this area in both PIOMAS model tuning and ICESat algorithm development.

[21] Applying the above derived biases (−0.01 and −0.26 m) from the ICESat domain to the full PIOMAS domain changes total Arctic sea ice volume estimates by −1.7 (i.e., −6.3%) and -2.3×10^3 km^3 (i.e., −10%) for spring and fall, respectively. Given the small number of data points (N = 5) involved in determining these biases, the uncertainty is of course large and conclusions about ice volume biases must be viewed with caution. Uncertainties in local and regional mean ice thickness are summarized in Table 1.

3.3. Uncertainty in Spatial Patterns

[22] ICESat-derived ice thickness fields also provide the opportunity to assess the fidelity with which PIOMAS integrations reproduce the spatial patterns of ice thickness. Difference maps were computed for each ICESat campaign and average differences computed for spring and fall (Figure 6). ICESat and PIOMAS ice thickness fields show a

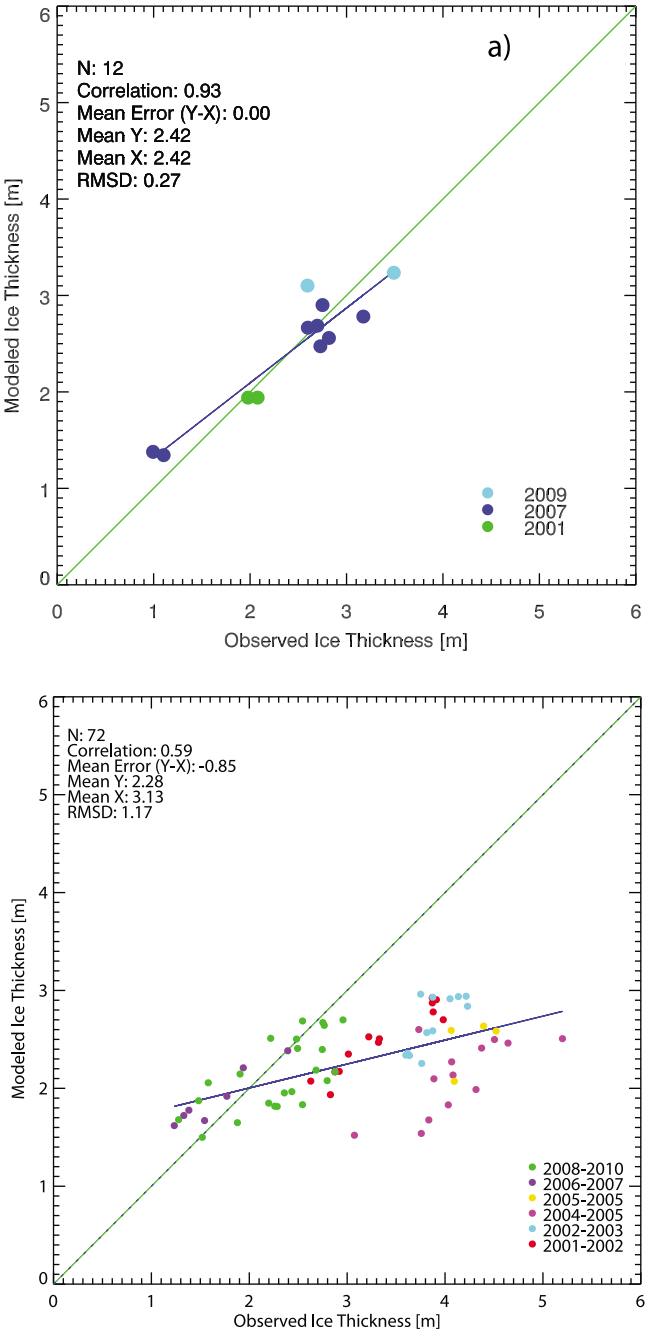

Figure 4. Comparison of PIOMAS (IC-SST) with in situ observations from the sea ice CDR from 1999 to 2010 (a) for EM measurements and (b) NPEO ULS measurements. Colors in Figure 4a refer to different measurement campaign years and in Figure 4b to years of deployment for NPEO ULS instruments.

close agreement with the overall pattern of ice thickness. Pattern correlations are high with values of 0.8 and 0.9 for spring and fall fields, respectively. The IC integration performs a bit worse than IC-SST and model only, consistent with comparisons against sea ice CDR observations. The largest differences in ice thickness patterns occur in a narrow band along the northern coast of Greenland and the Canadian Archipelago, where ice thicknesses are larger and meridional gradients much steeper in the ICESat data than in the PIOMAS model. At the current configuration with smooth, low-resolution forcing fields, PIOMAS seems to have trouble reproducing the thick ice along the coast, contributing to the negative bias noted above. This difference in spatial pattern serves as an explanation for the above noted regional mean ice thickness difference between PIOMAS and ICESat (Figure 5). However, while the underestimate of ice thickness near the Canadian coast is qualitatively supported by comparisons with near coastal observations from the sea ice CDR (Figure 7), PIOMAS underestimates are much smaller (0.08 m) than apparent from the ICESat comparison. It is possible that the ICESat retrievals may overestimate ice thickness along those coastal area. However, some of the EM data near Ellesmere Island also tend to show thicker ice than PIOMAS, pointing to potential model biases which suggest that additional work is needed to characterize ice thickness variability in those areas. PIOMAS ice thickness in the Beaufort and Chukchi Seas is somewhat thinner than observed from ICESat. Because it is derived for regional means, the correction of −0.20 m applied to the ICESat regional means to adjust October–November ICESat retrievals to the 1 November reference date as done for KR09 was not applied to the maps shown in Figure 6.

4. Ice Thickness Trends and Uncertainties

4.1. Comparisons With Reconstructed Time Series [KR09]

[23] So far we have examined local and regional uncertainties and differences in spatial patterns. What about long-term trends, the ultimate goal of this paper? To determine uncertainties in long-term trends, one needs to address the irregular spatial and temporal sampling of the available data. Satellite-derived records (ICESat) are still too short. RPW08 address in situ sampling issues by fitting an empirical model to available in situ data for the DRA and KR09 concatenate the ICESat record to construct a time series of mean ice thickness for the DRA. We use this time series to assess the corresponding long-term variability in PIOMAS ice thickness.

[24] Figure 8 shows PIOMAS ice thickness (IC-SST) averaged over the DRA and ice thickness time series from KR09. PIOMAS ice thickness is well within the error estimates of KR09, except for a period in the early 1980s. This discrepancy possibly arises from the higher-order polynomials utilized by RPW08 to interpolate submarine data in space and time.

[25] Figure 8a shows in situ observations from the sea ice CDR that were taken within the DRA over the January–May time window. There are no February–March observations for the 1981–1985 period, when the discrepancy between PIOMAS and the regression model occurs and the regression model fit appears to be influenced strongly by the fall observations. During that time, though still apparent, the discrepancy between PIOMAS and the regression model is substantially smaller. The scatter of individual CDR observations about their means illustrates the large spatial variability in ice thickness that makes the construction an Arctic-wide time series from sparse in situ observations so difficult. The

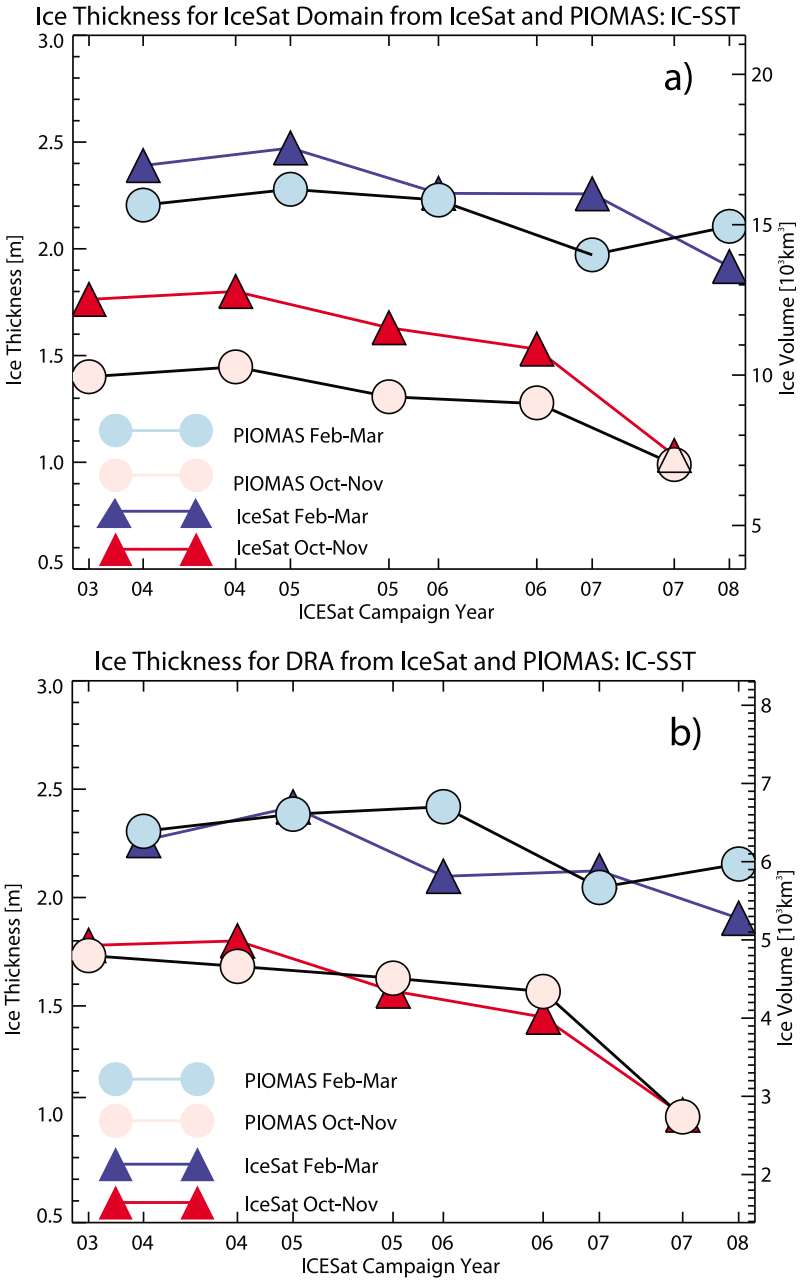

Figure 5. Comparison of ice thickness and volume for (a) entire ICESat domain from PIOMAS (IC-SST) and (b) for the DRA only.

differences between the sea ice CDR means and the regression model show the importance and difficulty of accounting for this sparse sampling as attempted by RPW08.

[26] KR09's stated uncertainty of 0.50 m is the standard deviation of the error of the regression model for monthly averaged ice thickness spatially averaged over the DRA. It can be interpreted as the expectation that 67% of observed monthly averages will lie within this bound. Given the length of the time series of 34 years and ignoring autocorrelation, one would then expect up to 11 years of data to lie outside this bound. Thus, even though several of the model data points in the early 1980s fall outside the error bounds of the KR09 time series, the ice thickness predicted by PIOMAS for the DRA is statistically consistent with the reconstructed KR09 time series. RMS differences between the PIOMAS (IC-SST) and the KR09 time series are 0.40 and 0.32 m for spring and fall, respectively, i.e., within the uncertainty of the KR09 thickness estimates. The mean bias is 0.17 m and near zero for spring and fall, respectively. However, PIOMAS model trends for the 1979–2010 periods are −0.25 and −0.38 m decade^{-1} for spring and fall for the IC-SST run, respectively. This contrasts with trends of −0.53 and −0.50 m decade^{-1} for the KR09 time series. Given the functional form underlying the KR09 time series a comparison of linear trends of the time series is probably not the best way to assess the agreement. Instead, the qualitative similarity of the time series may be a more useful indicator of agreement between model and observations.

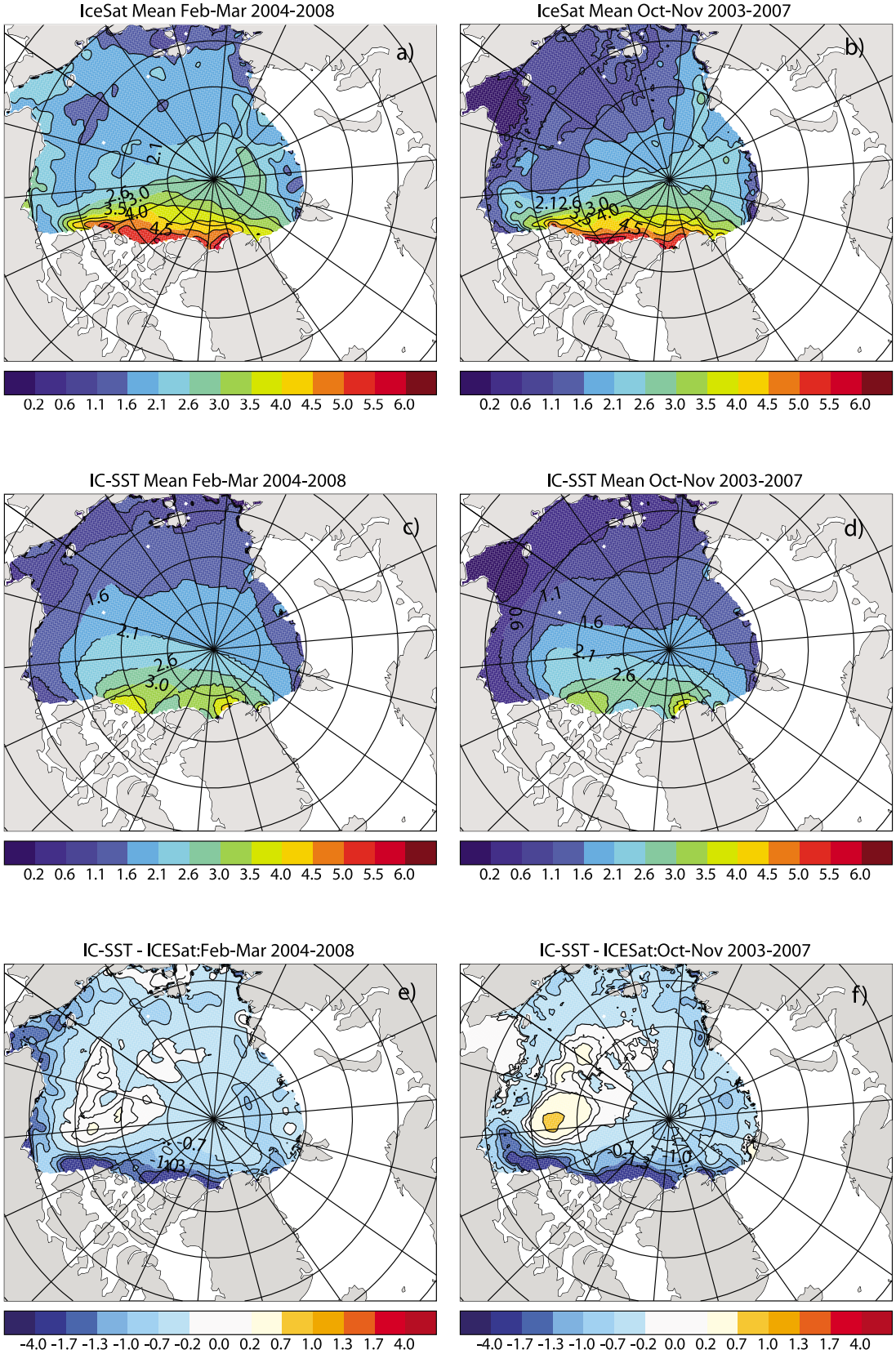

Figure 6. Mean 2003–2008 (a,b) ICESat and (c,d) PIOMAS ice thickness for February–March (Figures 6a and 6c) and October–November (Figures 6b and 6d). (e,f) Difference maps are shown. The color scale is given in m.

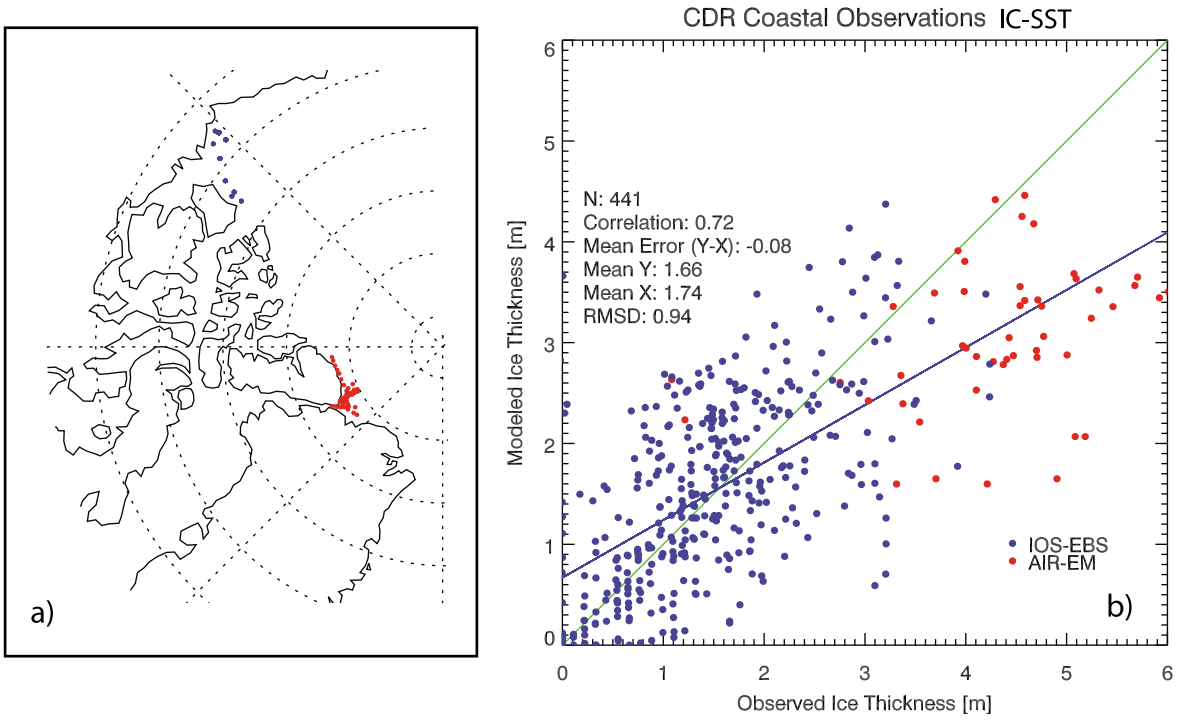

Figure 7. Comparison of PIOMAS (IC-SST) and airborne EM (AIR-EM) and moored ULS (IOS-EBS) measurements near Canadian coast. (a) Map of comparison locations. (b) Comparison with PIOMAS ice thickness. ULS measurements are from the IOS-EBS site.

[27] Large differences between PIOMAS and the in situ observations from the CDR are apparent in the gap between the regression model and the beginning of the ICESat period (2000–2003). These observations are from the NPEO which we have previously shown to have large biases relative to PIOMAS. The discontinuity of these observations relative to the PIOMAS and KR09 time series further raises questions about their validity. We need to however recognize that if the pre-2006 NPEO thickness estimates are indeed correct and representative for sea ice conditions during that period that our understanding of the variability of sea ice thickness and volume in the Arctic would be seriously challenged.

[28] Though KR09 provide no uncertainty estimate for their trends, those can be estimated to be in the order of 0.10 m decade^{-1} by specifying the uncertainties reported by KR09 as measurement errors in a linear fit procedure [e.g., *Press et al.*, 1992]. The difference in mean ice thickness trend between PIOMAS and KR09 is therefore outside the random uncertainties, thus pointing to the likelihood that systematic errors such as the previously noted tendency of PIOMAS to underestimate thick and overestimate thin ice accounts for the differences in trends. Both the IC and model-only runs show substantially larger thinning in the DRA region with October trends of −0.53 m decade^{-1}, thus being closer to the KR09 record. Our choice of IC-SST as our reference integration therefore clearly is conservative with respect to the trend.

4.2. Thickness Change From Paired Observations

[29] An alternative approach may also be taken to deal with the sparse spatial and temporal sampling of the observation. This approach assesses temporal change from observations for which repeat coverage exists at the same locations at same time of the year. *Rothrock et al.* [1999] and KR09 use this approach by grouping observations by location and period and calculate multidecadal trends for each of those location. Here we use a similar approach and compare modeled 10 year trends with observed 10 year trends at the same locations.

[30] We search the sea ice CDR database for pairs of repeat observations at the same location and time of the year (month) that are at least 10 years apart. Figure 9 shows the comparison of 10+ year trends from sea ice CDR observations and PIOMAS. Observations are paired regardless of the observation system. Naturally, the distribution of trends computed in this fashion is rather noisy, because observations reflect only small areas and two-point trends are strongly by affected by year-to-year variability. In addition pairs of observations may have different biases due to the nature of the measurements (e.g., deployment depth or measurement system). A total of $N = 572$ pairs yield a mean thickness change for PIOMAS of −0.42 m decade^{-1}. The observed mean decrease is somewhat larger with −0.48 m decade^{-1}. Using a T means test, we find that the mean trend for PIOMAS is significantly ($p < 0.003$) different from the mean thickness change obtained from the observations Based on this statistic we find that PIOMAS underestimates ice thickness decline by as much as 0.06 m decade^{-1}. Note however that previously discussed differences in measurement biases affect this finding. While the sampling of the paired observations precludes using the derived changes as a representative value for changes in basin-wide ice thickness over the period, the difference between model and observed trends (0.06 m decade^{-1}) maybe taken as an indication of the uncertainty of both estimates. This result provides further

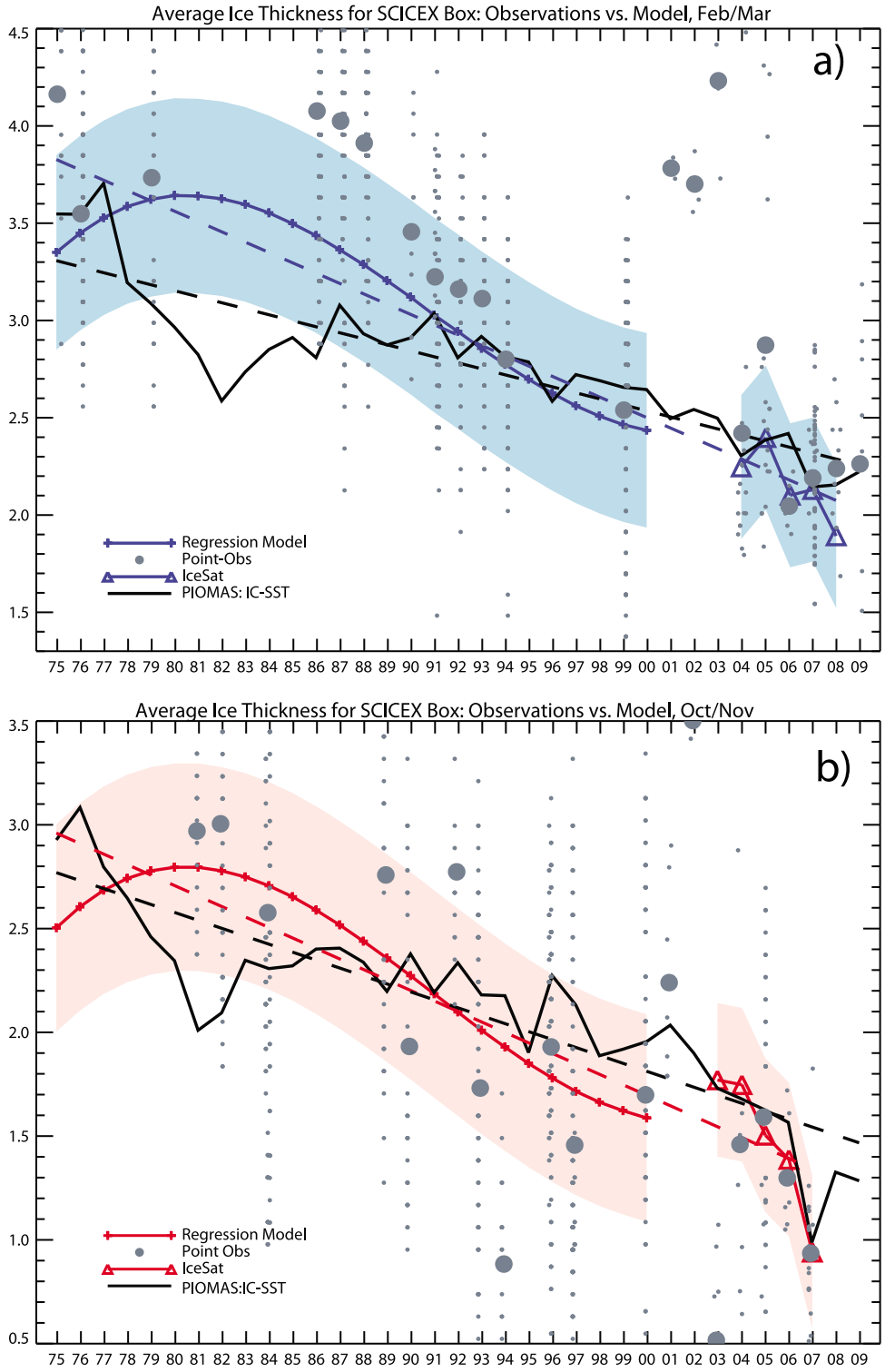

Figure 8. Comparison of PIOMAS model run (IC-SST) with the KR09 regression model constructed from U.S. submarines and the ICESat-based ice thickness for (a) February–March and (b) October–November. PIOMAS data are averages for the two months bracketing the ICESat campaigns. The regression model is evaluated for 1 March and 1 November. ICESat data for fall are corrected to 1 November by subtracting 0.20 m. Shaded areas represent uncertainties (1σ) estimated by KR09. Individual monthly observations from the sea ice CDR are shown as small gray dots. Large gray dots represent the mean of all observations for that time window. Dashed lines represent linear fits for PIOMAS (black dashed), and KR09 (blue dashed/red dashed). Observation means can substantially differ from the regression model because of the space-time weighting applied in constructing the regression model (see RPW08 for details).

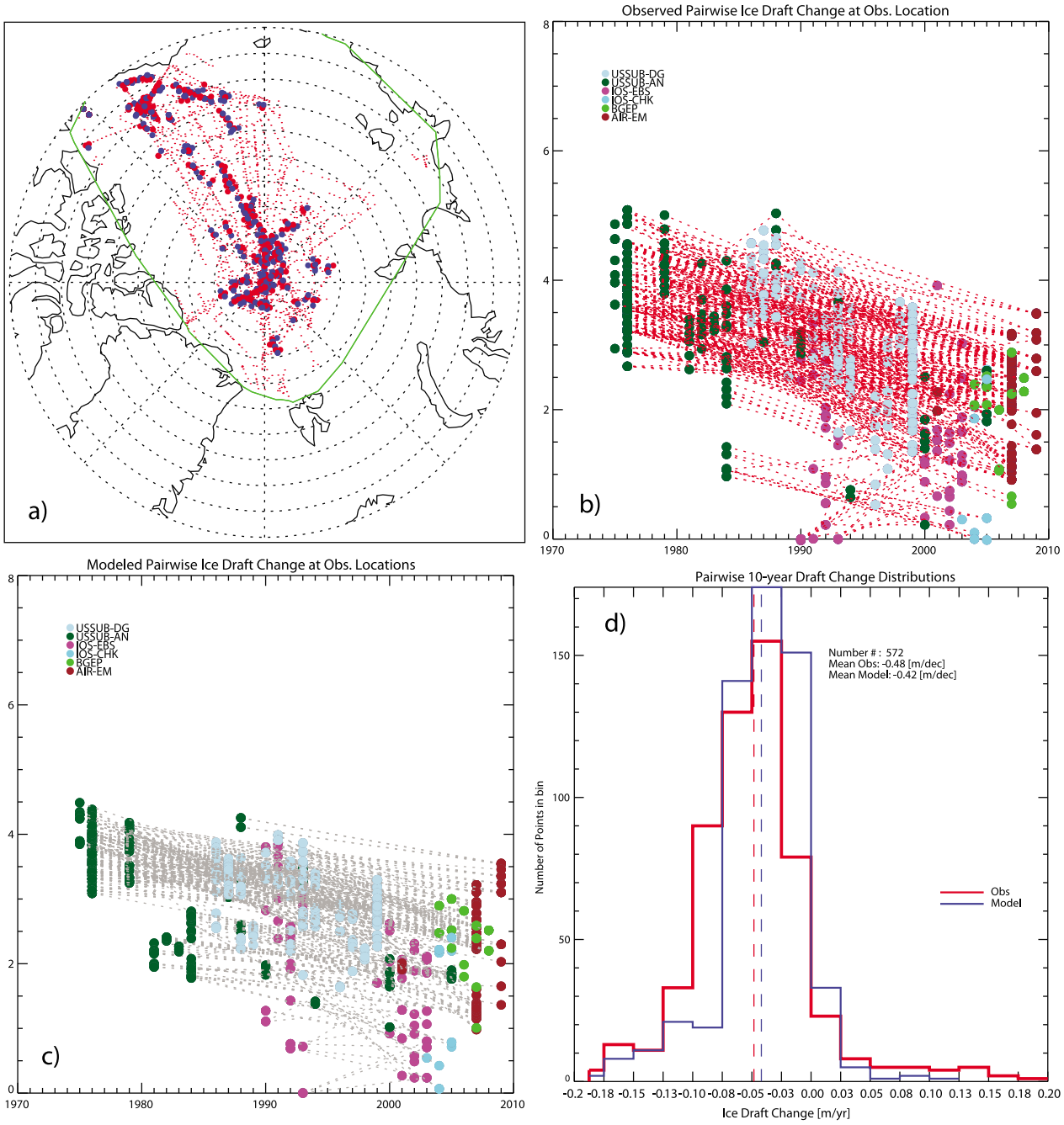

Figure 9. Comparison of 10+ year differences at repeat locations. (a) Locations, (b) differences for observations, (c) differences for PIOMAS, and (d) histograms of difference distributions for observations and the model are shown. Mean difference from observations is –0.48 m decade^{-1} and from PIOMAS is −0.42 m decade^{-1}. Locations of repeats are coded in different colors in Figure 9a to show the separation distance. Colors in Figures 9c and 9d indicate different sources of thickness information (see Figures 2 and 3). Dashed lines in Figure 9d are the means of the distributions for PIOMAS and observations.

evidence that PIOMAS yields a conservative estimate of changes in ice thickness.

5. Ice Volume Uncertainties and Trends

[31] Total Arctic sea ice volume can be written as $V = \Sigma\, h_i\, a_i$ where h_i is the mean thickness of sea ice (including open water) in grid cell i, a_i is the cell area, and the sum is over N cells. If the error variance of h_i is denoted by σ_h^2 (independent of i), and if the errors in h_i are uncorrelated with each other, then the error variance of V is given by $\sigma_v^2 = \sigma_h^2\, \Sigma\, a_i^2$. Defining the mean square grid cell area by $a^2 = (1/N)\, \Sigma\, a_i^2$, the error standard deviation of V is then given by $\sigma_v = \sqrt{N} a \sigma_h$ (equation (1)). The uncertainty in volume is proportional to the uncertainty in thickness σ_h, the RMS grid cell area a, and the square root of the number of grid cells N. The volume is

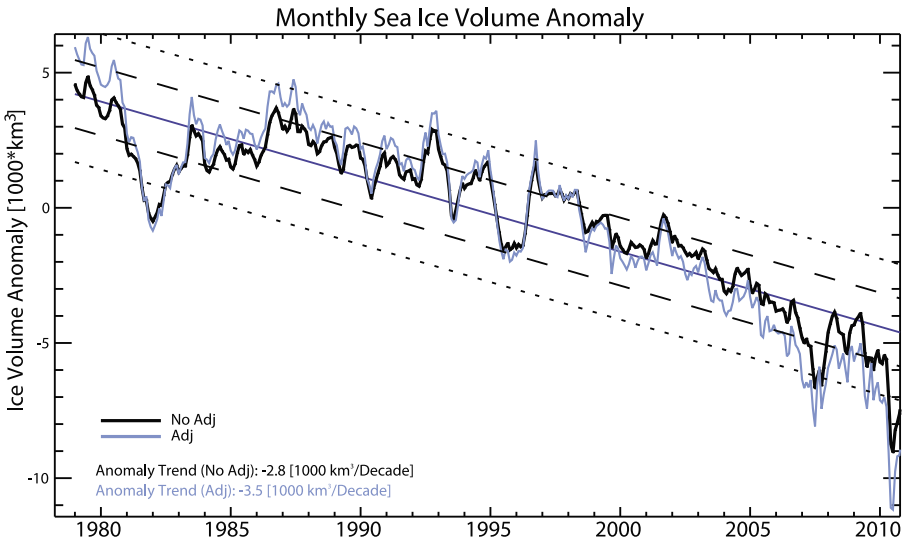

Figure 10. Adjusted and unadjusted monthly ice volume anomalies. Adjustments are calculated based on regressions between PIOMAS and observed ice thicknesses from the sea ice CDR.

affected by the definition of the domain as well as coastlines. The domain and grid are fixed for the PIOMAS, so a_i is a constant with time and will not impact the uncertainty of the time series. To obtain an estimate of the potential effect of coast line uncertainties we obtained the AMSR-E 6.25 km land mask from NSIDC. Comparing this mask with the PIOMAS grid, we estimate the total Arctic ice volume uncertainty due to coastline uncertainty to be less than 2% of total ice volume.

5.1. Volume and Trend Uncertainty From In Situ Thickness Observations

[32] The direct comparisons of observed ice thickness with PIOMAS integrations (section 3.1) yielded a maximum standard deviation of the difference between modeled and observed mean monthly ice thickness for each grid cell of 0.78 m and maximum bias of –0.17 m. Accounting for the varying PIOMAS grid spacing and the fact that a different number of grid cells are ice covered in March and October, we use equation (1) and set the grid cell uncertainty σ_h, to 0.78 m; N is set to the number of grid cells with a thickness greater than 0.15, we use the temporal mean (1979–2010) of 15,548 for March and 10,132 for October for N; the RMS grid cell area a is set to 1075 and 879 km^2 for March and October, respectively. The resulting random ice volume uncertainty for the entire PIOMAS domain is rather small: 0.1×10^3 km^3 for March and 0.07×10^3 km^3 for October. Much more significant is the impact of potential biases in ice thickness. By multiplying the established −0.17 m bias with the ice-covered areas for March and October, the volume bias is calculated. Over the PIOMAS domain, the modeled ice volume bias relative to the CDR with submarine data is -2.8×10^3 km^3 for March and -1.5×10^3 km^3 for October, or about 10% of the total ice volume at those times.

[33] Using above calculated ice volume uncertainty of 0.1×10^3 km^3 as the measurement error when calculating the trend [*Press et al.*, 1992] of the monthly volume anomaly yields an uncertainty of 0.07×10^3 km^3 decade^{-1} in the linear trend. This trend uncertainty needs to be viewed as rather optimistic since it is based on the assumption that errors are random. Biases, if assumed constant, do not affect the uncertainty of the volume trends. However, this assumption is likely not a good one. As shown in 3.1, comparisons with observations indicate that PIOMAS tends to overestimate the thickness of thin ice and underestimate the thickness of thick ice. In section 5.2 we will therefore attempt to quantify the impact of such systematic errors on ice volume trends.

5.2. Uncertainty Using Adjusted Model Output

[34] As previously discussed, the comparison of PIOMAS results with thickness observations, assuming that those are free of systematic errors, shows that the model appears to overestimate thin ice and underestimate thick ice (Figure 2). How do such systematic differences impact ice volume trends? To answer this question, we transform modeled ice thickness to an "adjusted" ice thickness that removes such differences. We estimate linear coefficients for $h_{obs} = a + b*h_{Model}$ using all in situ observations using a procedure that allows for errors in both dependent and independent variables [*Williams et al.*, 2010]. Making the assumption that this relationship holds everywhere and at all times, we apply the resulting coefficients to individual PIOMAS grid cells and then sum spatially to recompute time series of ice volume anomalies.

[35] The results (Figure 10) show that anomalies are relatively insensitive to this correction but that the downward trend is somewhat increased. Because thick ice in the earlier period increases in thickness, and thinner ice during the later period is thinned by this adjustment, the downward decadal trend increases from -2.8 to -3.5×10^3 km^3 decade^{-1}. Mean total ice volume over the 1979–2010 period decreases from 21 to 19 $\times 10^3$ km^3. Note that this exercise is not designed to correct potential model biases, nor do we discount the possibility that model and observational differences are due to errors in the observations. It does however provide a measure of the sensitivity of ice volume estimates to the noted systematic differences between modeled and observed ice thickness. Using the change in trends as a measure of

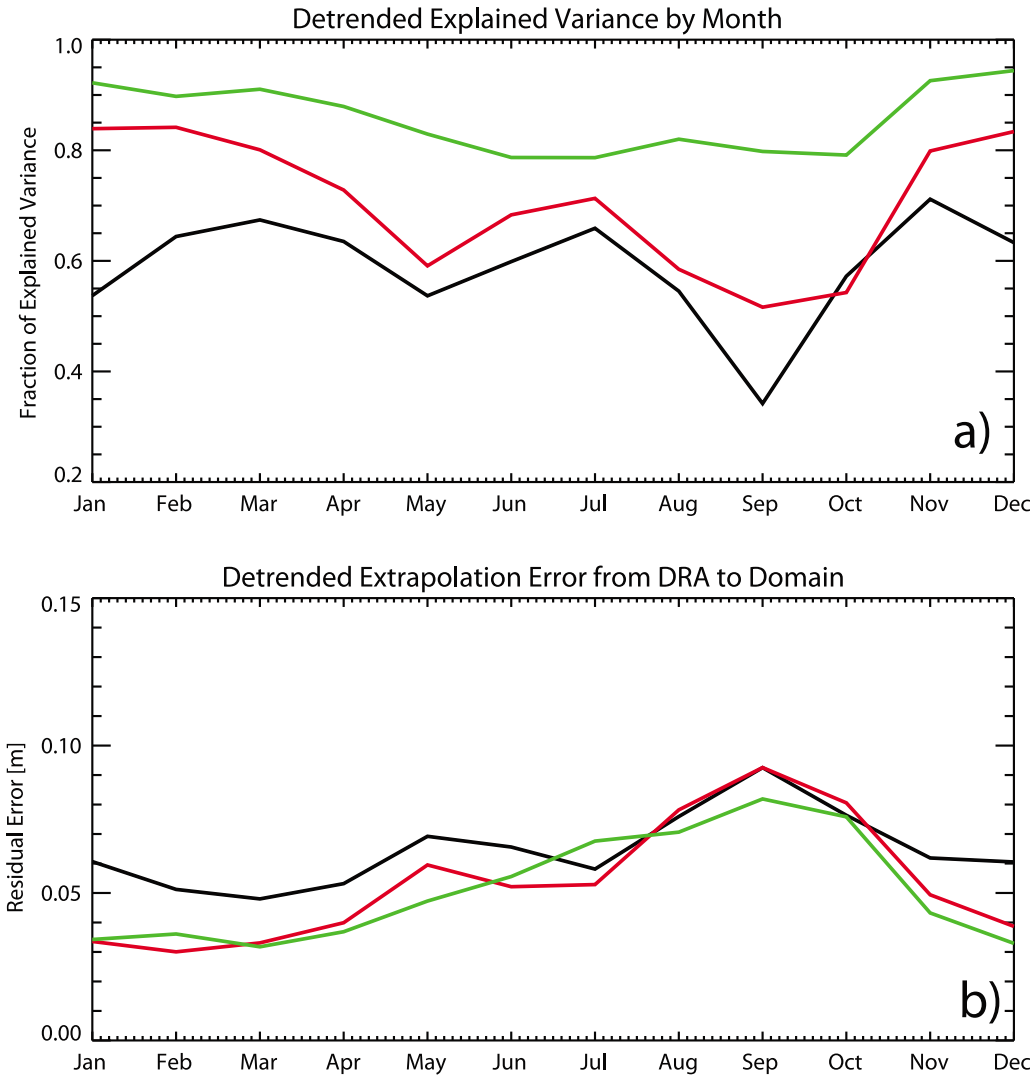

Figure 11. Monthly detrended regression of the mean monthly ice volume for the DRA on ice volume over the entire PIOMAS domain (a) explained variance r^2 and (b) residual error of regression or "extrapolation error." Green line is model only, black line is IC, and red line is IC-SST.

uncertainty, we arrive at a value of the trend uncertainty of 0.7×10^3 km^3 decade^{-1}. The standard deviation of the difference between the unadjusted and the adjusted volume anomalies is 0.76×10^3 km^3 which can be viewed as an indicator of the uncertainty of the individual monthly volume estimates.

5.3. Extrapolation Error

[36] At this point we have assessed PIOMAS uncertainties from direct observations, interpolated (regressed) submarine ULS data, and ICESat measurements. We showed that PIOMAS performance appeared slightly worse for the entire ICESsat domain than for the DRA only. Beyond the comparison with ICESat, little is known about ice thickness uncertainty outside the DRA.

[37] In order to gain insight into how well sea ice thickness variability inside the DRA relates to sea ice thickness variability in the entire Arctic (PIOMAS domain), we correlate PIOMAS ice thickness averaged for the DRA with average ice thickness for the entire domain for each month of the year (Figure 11). For the purpose of this calculation mean ice thickness is calculated using a minimum thickness threshold of 0.15 m. Both time series are detrended to remove the correlation due to the long-term trend. Making the assumption that the relationship between PIOMAS ice thickness for the DRA to the PIOMAS domain average reflects reality, we can estimate the potential error incurred by estimating total Arctic ice thickness from DRA averages. The explained variance values range from 32% to 95% depending on the model version and the month. Note that the model-only integration, which does not use assimilation, shows little seasonal variation in the amount of explained variance. In contrast, the IC-SST and IC integrations which assimilate data to constrain the model have lower values of explained variance, particularly in spring and fall. This suggests that the assimilation process introduces a substantial amount of variance into the ice thickness outside the DRA and that ice thickness variability outside the DRA is much less controlled by the dynamics and thermodynamics captured by the model and forcing data than in the DRA.

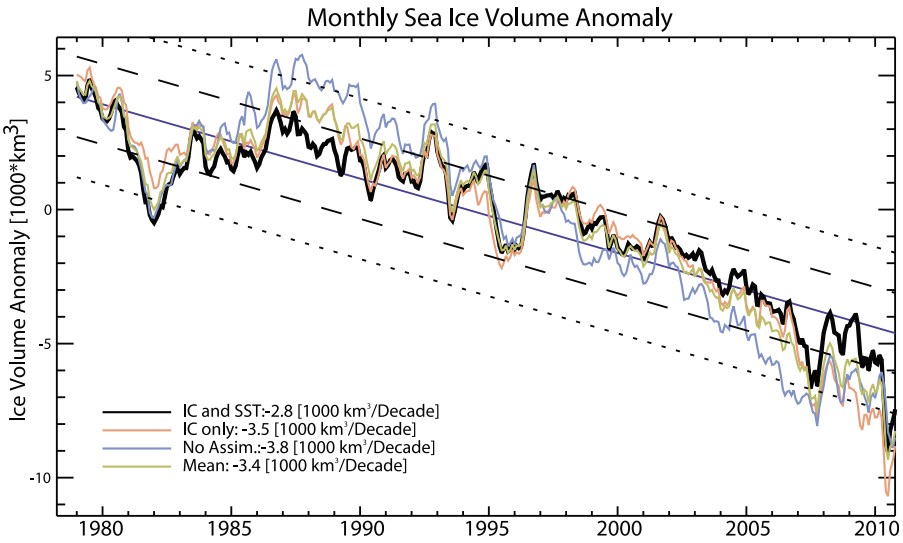

Figure 12. Monthly ice volume anomalies from three different PIOMAS integrations. Anomalies are computed relative to the 1979–2009 period. The 1979–2010 linear trends for different model runs and for the multirun mean are given in the legend.

PIOMAS is apparently getting significant help from the assimilation procedure. Future model development and thickness measurement campaigns should therefore focus on areas outside the DRA. Note however, that in PIOMAS assimilation runs, at least 50% (except for September) of the variance of the volume over the entire domain is still explained by the ice thickness in the DRA. Thus, the mean thickness error incurred by estimating Arctic-wide ice thickness from DRA values, estimated as the residual error of the regression shown in Figure 11b, is relatively small (<0.1 m).

[38] Using the ice-covered area of the PIOMAS domain outside the DRA to convert this thickness extrapolation uncertainty into a volume uncertainty yields an additional volume uncertainty of 0.63×10^3 km^3 for October. Noting the previously established volume uncertainty of 0.1×10^3 km^3 based on CDR data for the DRA, we can see that the random volume uncertainty for the PIOMAS domain is dominated by this extrapolation error. This analysis assumes that the model captures the natural correlation of ice thickness covariability between the DRA and the entire PIOMAS domain, which is of course unproven since little data exist which would allow systematic evaluation.

5.4. Volume Uncertainty From Different PIOMAS Runs

[39] In sections 5.1–5.3, we assessed modeled ice volume uncertainties through comparisons with observations. Given uncertainties in sampling and data quality, it appears prudent to further support the results through model sensitivity studies. Here we compare three different PIOMAS integrations and examine the range of ice volume and anomaly estimates and linear ice volume trends. Integrations of PIOMAS using different parameters for ice strength and using different inputs for assimilation are compared. This approach follows the perturbed physics approach [e.g., *Sanderson et al.*, 2008] to estimating uncertainty in climate model projections. However, in contrast to perturbed physics experiments which create an ensemble of integrations from which uncertainty with respect to a particular parameter can be estimated, we here select three experimental integrations that have evolved over time and provide similarly good validation statistics when compared to submarine ice draft data. The differences between these runs can be considered one measure of the model uncertainty as it represents the sensitivity of ice volume estimates to a subset of "reasonable" choices. Reasonable in this context is defined as meeting specific validation criteria such as explained variance and mean of observed ice draft. As discussed in section 2.1 differences between the IC-SST and IC are in part due to SST assimilation, in part due to a different choice in ice strength parameterization [*Steele et al.*, 1997].

[40] Figure 12 shows the monthly ice volume anomaly relative to the 1979–2009 mean from the three integrations. Resulting volume anomaly trends for the period 1979–2010 range from -2.8×10^3 km^3 decade^{-1} for the run assimilating ice concentration and SST (IC-SST) to -3.8×10^3 km^3 decade^{-1} for the run without assimilation (model only) with a mean trend over all integrations of trend -3.4×10^3 km^3 decade^{-1}. The uncertainty in the ice volume anomaly, estimated as the time averaged standard deviation of the three runs about the three-run mean anomaly, is 0.76×10^3 km^3. Individual runs differ in mean volume by as much as 3.8×10^3 km^3 in March and 2.4×10^3 km^3 in October. Time averaged standard deviations about the three-run volume mean are 2.25 and 1.35×10^3 km^3 for March and October, respectively, and provide one measure of the total ice volume uncertainty. These differences arise largely from the fact that the no assimilation run (model only) has significantly larger ice volume throughout the period. Volume anomaly uncertainties estimated in this fashion are substantially smaller than for the total volume because individual model biases are removed when the anomalies are computed.

[41] Which run is better? What is the actual trend? How can we estimate an uncertainty of ice volume and trends from these different integrations? There is of course no simple answer to these questions. Both model-only and IC-SST runs have nearly identical validation statistics when compared

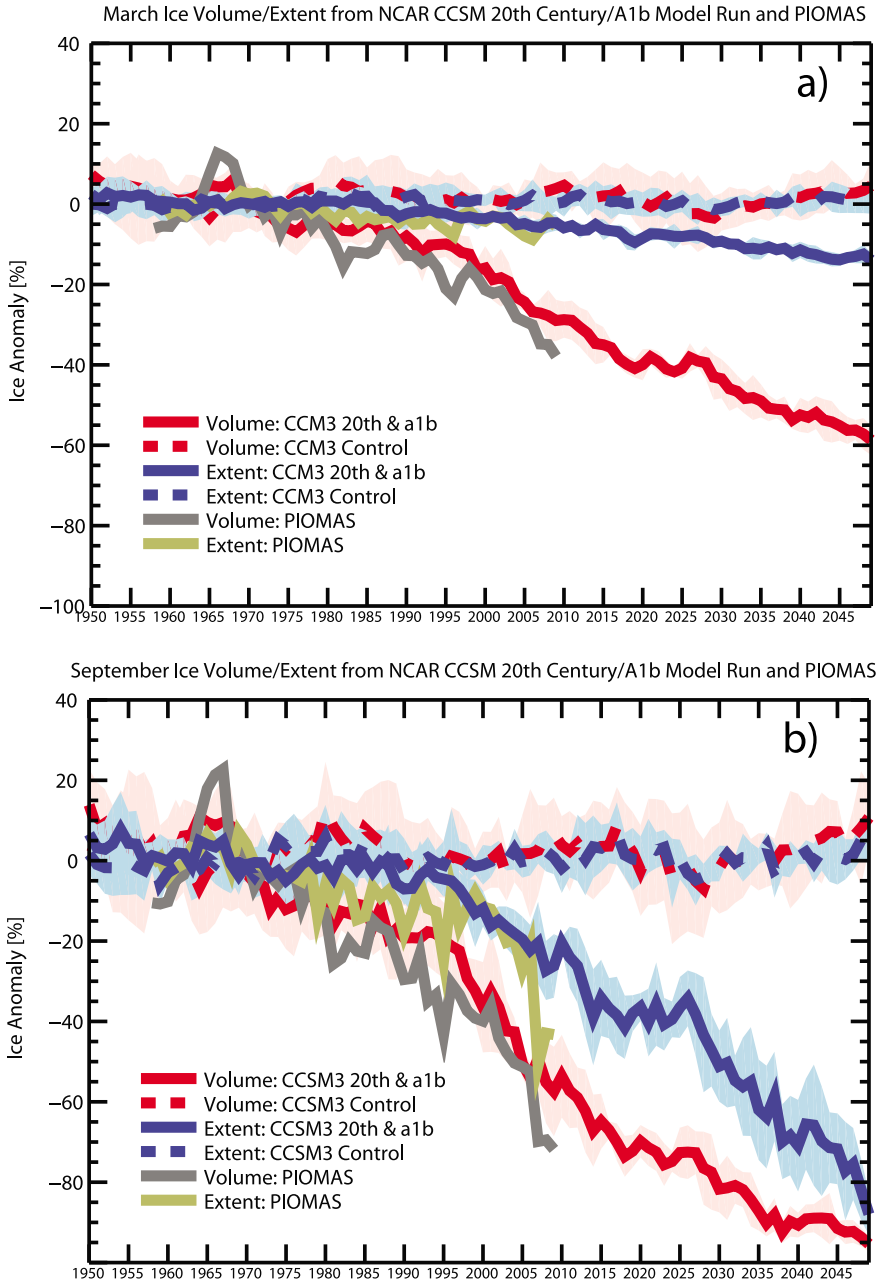

Figure 13. Fractional ice volume and extent anomalies relative to 1958–1978 from PIOMAS (IC) and CCSM3 combined 20th century and A1b scenario ensembles and preindustrial control ensemble for (a) March and (b) September. Shaded areas indicate the standard deviation about the ensemble mean for the CCSM3 ensembles.

with in situ ice thickness observations, though the mean difference between those runs is largest where there are few validation data. Both ice concentration-only (IC) and no assimilation (model only) runs have long-term trends that compare more favorably with the concatenated time series of KR09. Both assimilation runs constrain the ice concentrations to observations and therefore provide a more accurate representation of ice extent and concentration. So what do we do? Until further improvements in models and observations allow us to clearly identify the "best" model integration, it appears reasonable, particularly for climate change detection and attribution questions, to select the integration with the most conservative estimate for the trend (-2.8×10^3 km^3 decade^{-1}) as our "reference" integration and use the range in trends (1.0×10^3 km^3 decade^{-1}) as an indicator of potential uncertainty.

6. Applications

6.1. Comparisons of PIOMAS and CCSM3 Ice Volume and Extent Change

[42] To put the uncertainty estimate for ice volume trend into context we compare PIOMAS-derived ice thickness trends with those derived from the NCAR Community

Climate System Model V3. Northern Hemisphere ice volume and ice extent anomalies from the 20th century run (20C3M) and A1b scenario runs are computed for five realizations. Anomalies are computed relative to the 1958–1978 period and are expressed as percentages of the total ice volume or ice extent for the period. Five hundred years from the preindustrial control run are used to create a five-member pseudoensemble to represent internal variability.

[43] Figure 13 shows the fractional anomalies for ice extent and ice volume from the NCAR CCSM3 model runs and PIOMAS for September and March. The PIOMAS IC run is used in this case instead of the reference IC-SST run since the IC-SST starts after 1975 because of a lack of SST data. In both seasons, ice volume anomalies begin to separate from the control run earlier than ice extent anomalies. During the winter season, when the ice extent is in part controlled by geography, the separation between the volume and extent lines is larger and continues to grow through 2050. In the fall seasons, relative ice volume and ice extent losses narrow toward the end of the period when little ice remains. Both the PIOMAS and the CCSM3 simulations suggest that the ice volume compared to extent is an earlier indicator of the decline of the ice pack by very roughly 10–15 years. The noisy nature of the simulations precludes a precise determination. By the mid-1990, ice volume losses in September exceed ice extent losses by a factor of 4 in both PIOMAS and CCSM3. As the ice thins further, ice extent losses accelerate relative to volume losses until volume/extent anomaly ratios are near one by 2050.

[44] Accepting PIOMAS ice volume and ice extent losses as a proxy for reality, it appears that CCSM3 hindcast/projection matches rather well. Ice volume and extent losses stay within or are close to the bottom edge of the envelope established by the ensemble for most of the time since significant ice losses began in about 1988. This is the time when the Arctic Oscillation started a strongly positive phase for a few years before returning to more normal conditions [*Lindsay and Zhang*, 2005]. The exception is since 2007 when ice extent and to a lesser degree the ice volume dropped significantly below the CCSM3 envelope in the fall. This observation contrasts with the frequently made statement that global climate models do not capture the observed trend in ice extent over the 1953–2006 period [*Stroeve et al.*, 2007]. As shown in their paper and reiterated here with respect to ice volume trends, more sensitive climate models such as the NCAR CCSM3 and Hadley Center HadGEM1 models have 1979–2006 ice extent and volume trends that are quite comparable to observed (PIOMAS proxy) trends. Thus, If we accept this match as a measure of how well global climate models produce sea ice variability, then the state of the art is significantly better than apparent from a multimodel ensemble that includes many models with much less sophisticated sea ice representations.

[45] Figure 14a shows the ice extent anomalies (km^2) versus the ice volume anomalies (km^3) for a subset of IPCC AR4 models deemed to be more realistic based on their annual cycle and mean ice extent [*Wang and Overland*, 2009] (see Table 5 for abbreviations). All models lose ice extent and volume over time, but models with initially greater, more realistic sea ice volumes (such as NCAR CCSM3) lose ice extent more slowly than models with initially smaller sea ice volumes (such as ECHO-G or CNRM). In all cases, as the ice thins, the ice extent loss accelerates.

[46] The ice extent anomalies ($E - E_0$) and ice volume anomalies ($V - V_0$) are departures from reference values E_0 and V_0, which are different for every model. If instead we use fractional ice extent (E/E_0) and fractional ice volume (V/V_0), all the models coalesce onto a single curve (Figure 14b) of the form: $E/E_0 = 1 + 0.3*ln(V/V_0)$. This logarithmic relationship is related to the open water formation efficiency (OWFE) of [*Holland et al.*, 2006; *Merryfield et al.*, 2009], which is defined as the fractional change in open water per meter of vertical ice melt. *Merryfield et al.* [2009] found that OWFE is proportional to 1/(mean ice thickness) for a CCSM3 A1B simulation through 2100. Taking the derivative of our logarithmic relationship with respect to V shows that dE/dV is proportional to $1/V$, which is essentially the same as Merryfield's OWFE relationship, because sea ice volume per unit area is the same as mean ice thickness. The relationship between extent and volume follows from the sea ice thickness distribution, which evolves with a seasonal cycle. The selection of models based on their seasonal cycle is a possible explanation for the similarity of the ice extent/volume relationship in all the models. A more detailed discussion of these topics will be given by H. Stern et al. (The relationship between sea ice extent and volume, manuscript in preparation, 2011).

6.2. Attribution of Ice Volume Loss to Anthropogenic Greenhouse Forcing

[47] We now address the question how uncertainties in ice volume affect the attribution of changes in ice loss due to anthropogenic factors. In order to do this we employ a bootstrap method [*Vinnikov et al.*, 1999] to establish the probability that an observed (or proxy) trend could be found in a control climate without changes in anthropogenic greenhouse gas forcing.

[48] Figure 15 contrasts the 32 year trend distribution (1979–2010) in the NCAR CCSM3 preindustrial control run (500 years), compared with the trends from PIOMAS and CCSM3 20C3M/A1b runs. Based on this distribution, there is a negligible probability that a trend of the observed (PIOMAS) magnitude occurs without anthropogenic forcing. Using an uncertainty for the observed trend of 1×10^3 km^3 $decade^{-1}$, and an upper bound (-1.8×10^3 km^3 $decade^{-1}$) for ice volume loss, increases the probability to 0.01%. Since our choice of the IC-SST run is already conservative with respect to the downward trend, and there are numerous indications that the actual trend is larger, this upper bound appears extremely unlikely. Making the assumption that the preindustrial control run reflects the internal variability of the system properly, it is very unlikely that a trend in ice volume as obtained by PIOMAS, even accounting for large potential errors, would have occurred without anthropogenic forcings. Accepting the close match between CCSM3 and PIOMAS ice volume losses as evidence that CCSM3 provides a realistic sea ice sensitivity to climate forcing, we conclude that the attribution of ice volume loss to changes in anthropogenic greenhouse gases is not sensitive to the errors in observed ice volume losses. We emphasize that this exercise is not designed to resolve the issue of attribution but rather to examine the sensitivity of attribution to uncertainty of ice volume observations.

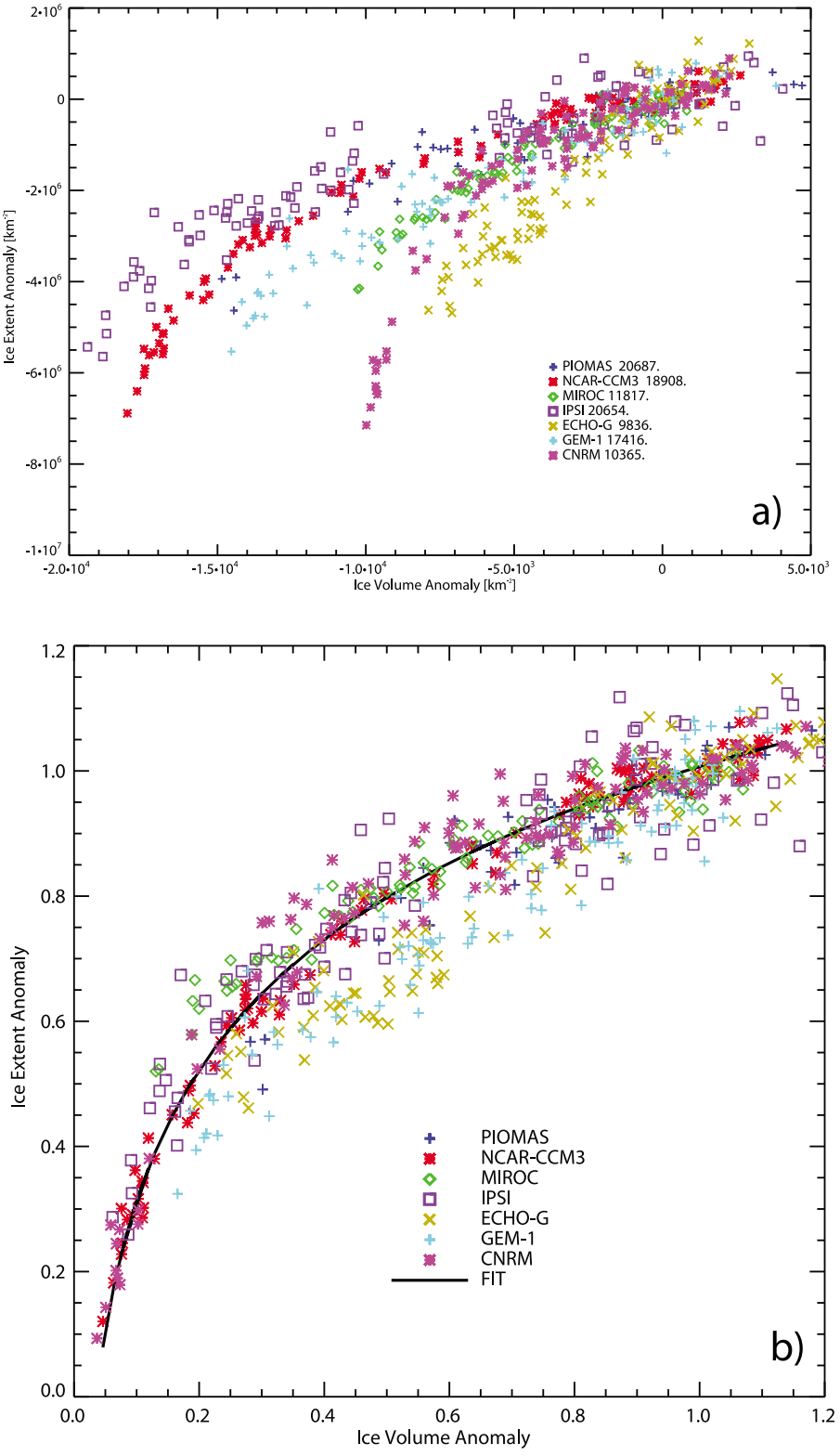

Figure 14. (a) Ice volume anomaly versus ice extent anomaly from PIOMAS and a subset of CMIP3 models. Anomalies are computed for each model relative to the 1958–1978 mean ice volume for the 1958–1978 period, which is given in km^3 in the legend following the name of the model. (b) Same as in Figure 14a but volume and extent anomaly are plotted as fractions of the 1958–1978 mean. Definition of model abbreviations can be found in Table 5.

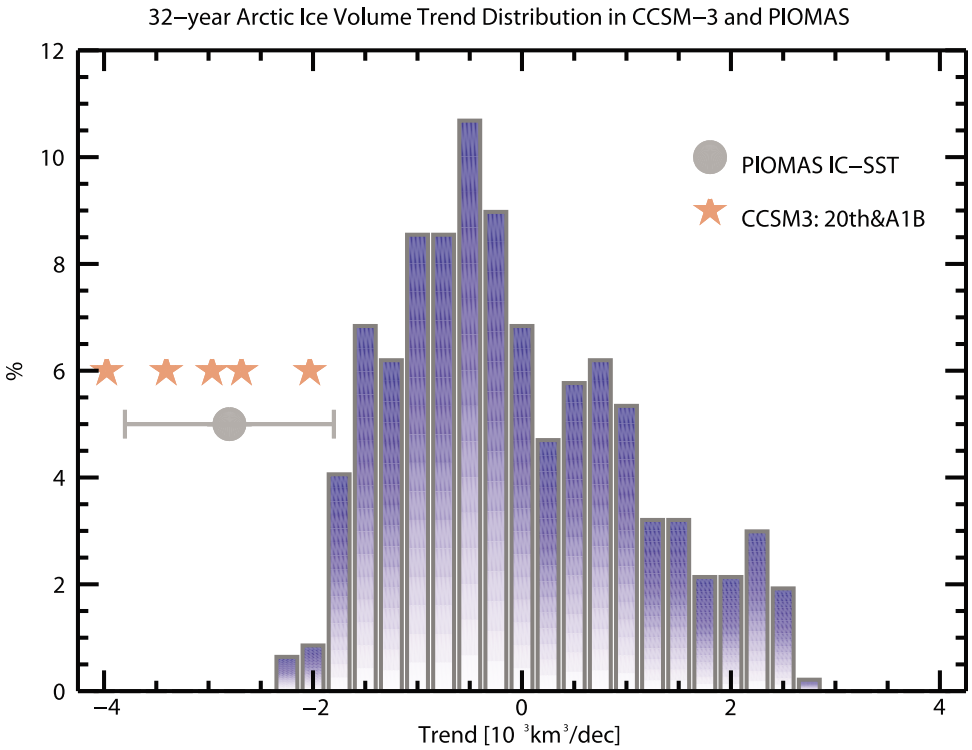

Figure 15. Distribution of 32 year trends in ice volume in the CCSM3 500 year control run (blue bars). Trends from PIOMAS along with extreme error bounds (1×10^3 km^3 decade^{-1}) are plotted (gray dot and error bars). Also trends from the 20th century/A1b ensemble members are shown (stars).

6.3. Is It a Record?

[49] We are often asked whether a particular year represents a new record in ice volume. For example, during the fall of 2010, PIOMAS-derived September ice volume was at a minimum during the 32 year period for which we provide the anomaly. To assess how our established uncertainty affects whether any particular year constitutes a "record" minimum, we examine the time series of minima in the PIOMAS ice volume time series and compare them to the established maximum uncertainty for monthly ice volume of 1.35×10^3 km^3 . Only about 25% of new September minima exceed the previous minimum by more than this uncertainty. Using the 0.76×10^3 km^3 uncertainty for the anomaly time series, this number rises to 33%. These numbers underline the difficultly of establishing "records" from this time series. Using the strict 1.35×10^3 km^3 uncertainty criteria, however, 2010 establishes a new record relative to the previous 2007 record.

7. Summary and Conclusions

[50] Using a number of different approaches we have attempted to characterize the uncertainty in the PIOMAS Arctic ice volume record. Even though the results deliver a spectrum of possible uncertainties, showing how uncertainties are uncertain themselves, it appears possible to provide conservative estimates that bound the potential error.

[51] Mean ice thickness uncertainty for the DRA is 0.78 m (RMS) but biases as large as 0.4 m exist. In general PIOMAS, relative to observations, appears to overestimate the thickness of thin ice and underestimate the thickness of thick ice. Such systematic differences will affect long-term trends in thickness and volume. PIOMAS ice thickness agrees well (<0.1 m mean difference) with ICESat ice thickness retrievals for the DRA. Agreement in spatial thickness patterns between PIOMAS and ICESat is very good with pattern correlations of above 0.8. ICESat retrievals outside the DRA are considerably thicker (0.4 m mean) than PIOMAS simulations. This difference arises in part from the fact that ICESat retrievals along the northern coast of Greenland and the Canadian Archipelago are considerably thicker (0.7 m) than PIOMAS integrations. However, model comparisons with in situ observations in these areas show a much better agreement, suggesting that ICESat thickness estimates may be too high, though additional study of this issue is warranted. We further find that detrended ice thickness estimates for the DRA correlate highly with areas outside the DRA (r ~0.8), although PIOMAS does not capture some of the variability outside the DRA when run without assimilation. Considering that substantial total ice volume uncertainties arise from areas outside the DRA where a large fraction of in situ measurements are located, a renewed effort for additional measurement campaigns and modeling efforts appears warranted.

[52] What about multiyear trends? Our reference integration, a model run that assimilates SST and ice concentrations shows the mean monthly ice volume anomaly decreases by -2.8×10^3 km^3 decade^{-1} over the period 1979–2010. However, from comparisons with in situ observations, ICESat retrievals, and alternate model experiments, we have good reason to believe that this estimate is conservative and that actual downward trends are larger. Using the range between

different integration as a measure of uncertainty, we arrive at a conservative uncertainty estimate of 1×10^3 km^3 decade^{-1}.

[53] The uncertainty estimates stated throughout this paper show considerable range. The spatial and temporal sampling and the unknown systematic errors of the measurement systems preclude more definite uncertainty estimates. Further work will need to attempt to better characterize the measurement biases that may exists for each platform, and to examine systematic modeling errors that may have spatial and temporal variability. For many purposes, however, conservative estimates established here may suffice. Two examples are discussed here and may provide guidance for other applications.

[54] PIOMAS ice volume uncertainties and trends were examined in the context of climate change attribution and the declaration of record minima. Ice volume losses in CCSM3 integrations compare well with PIOMAS trends. We find no trends of similar magnitude in the distribution of 32 year trends in the preindustrial control simulation. We therefore conclude that attribution studies using models with similar sea ice sensitivities and internal variability as the CCSM3 are not likely to be affected by uncertainties in observed (proxy) ice volume anomaly trends. Attempts to label new September minima as new records are significantly more susceptible to modeling error. Assuming stationarity, the likelihood of establishing a "new record" that passes a stringent examination of uncertainty is less than 25%. However, the 2010 September ice volume anomaly did in fact exceed the previous 2007 minimum by a large enough margin to declare it a new record.

[55] **Acknowledgments.** This research was supported by grants from NASA's Cryosphere Sciences Program, the Arctic Section of the Office of Polar Programs at NSF, and NOAA. Individual investigators contributed their in situ data sets to the sea ice CDR. Their tremendous contribution in collectively establishing an in situ measurement network that provides the critical data to conduct a study at the present needs to be highlighted. Dick Moritz is thanked for contributing NPEO data and many useful discussions. We acknowledge the modeling groups, the Program for Climate Model Diagnosis and Intercomparison (PCMDI) and WCRP's Working Group on Coupled Modeling (WGCM) for their roles in making available the WCRP CMIP3 multimodel data set. Support of this data set is provided by the Office of Science, U.S. Department of Energy. NOAA Physical Science Division is thanked for providing model NCEP forcing data.

References

Eisenman, I. (2010), Geographic muting of changes in the Arctic sea ice cover, *Geophys. Res. Lett.*, *37*, L16501, doi:10.1029/2010GL043741.

Giles, K. A., S. W. Laxon, and A. L. Ridout (2008), Circumpolar thinning of Arctic sea ice following the 2007 record ice extent minimum, *Geophys. Res. Lett.*, *35*, L22502, doi:10.1029/2008GL035710.

Gregory, J. M., P. A. Stott, D. J. Cresswell, N. A. Rayner, C. Gordon, and D. M. H. Sexton (2002), Recent and future changes in Arctic sea ice simulated by the HadCM3 AOGCM, *Geophys. Res. Lett.*, *29*(24), 2175, doi:10.1029/2001GL014575.

Haas, C., J. Lobach, S. Hendricks, L. Rabenstein, and A. Pfaffling (2009), Helicopter-borne measurements of sea ice thickness, using a small and lightweight, digital EM system, *J. Appl. Geophys.*, *67*(3), 234–241, doi:10.1016/j.jappgeo.2008.05.005.

Haas, C., S. Hendricks, H. Eicken, and A. Herber (2010), Synoptic airborne thickness surveys reveal state of Arctic sea ice cover, *Geophys. Res. Lett.*, *37*, L09501, doi:10.1029/2010GL042652.

Hibler, W. D. (1979), Dynamic thermodynamic sea ice model, *J. Phys. Oceanogr.*, *9*(4), 815–846, doi:10.1175/1520-0485(1979)009<0815:ADTSIM>2.0.CO;2.

Hibler, W. D. (1980), Modeling a variable thickness sea ice cover, *Mon. Weather Rev.*, *108*(12), 1943–1973, doi:10.1175/1520-0493(1980)108<1943:MAVTSI>2.0.CO;2.

Holland, M. M., C. M. Bitz, and B. Tremblay (2006), Future abrupt reductions in the summer Arctic sea ice, *Geophys. Res. Lett.*, *33*, L23503, doi:10.1029/2006GL028024.

Intergovernmental Panel on Climate Change (2007), *Climage Change 2007: The Physical Science Basis: Working Group I Contribution to the Fourth Assessment Report of the IPCC*, edited by S. Solomon et al., Cambridge Univ. Press, New York.

Kalnay, E., et al. (1996), The NCEP/NCAR 40-year reanalysis project, *Bull. Am. Meteorol. Soc.*, *77*(3), 437–471, doi:10.1175/1520-0477(1996)077<0437:TNYRP>2.0.CO;2.

Kwok, R., and G. F. Cunningham (2008), ICESat over Arctic sea ice: Estimation of snow depth and ice thickness, *J. Geophys. Res.*, *113*, C08010, doi:10.1029/2008JC004753.

Kwok, R., and D. A. Rothrock (2009), Decline in Arctic sea ice thickness from submarine and ICESat records: 1958–2008, *Geophys. Res. Lett.*, *36*, L15501, doi:10.1029/2009GL039035.

Kwok, R., G. F. Cunningham, M. Wensnahan, I. Rigor, H. J. Zwally, and D. Yi (2009), Thinning and volume loss of the Arctic Ocean sea ice cover: 2003–2008, *J. Geophys. Res.*, *114*, C07005, doi:10.1029/2009JC005312.

Lindsay, R. W. (2010), New unified sea ice thickness climate data record, *Eos Trans. AGU*, *91*(44), 405–416, doi:10.1029/2010EO440001.

Lindsay, R. W., and J. Zhang (2005), The thinning of Arctic sea ice, 1988–2003: Have we passed a tipping point?, *J. Clim.*, *18*(22), 4879–4894, doi:10.1175/JCLI3587.1.

Lindsay, R. W., and J. Zhang (2006), Assimilation of ice concentration in an ice-ocean model, *J. Atmos. Oceanic Technol.*, *23*(5), 742–749, doi:10.1175/JTECH1871.1.

Manda, A., N. Hirose, and T. Yanagi (2005), Feasible method for the assimilation of satellite-derived SST with an ocean circulation model, *J. Atmos. Oceanic Technol.*, *22*(6), 746–756, doi:10.1175/JTECH1744.1.

Maslanik, J. A., C. Fowler, J. Stroeve, S. Drobot, H. J. Zwally, D. Yi, and W. Emery (2007), A younger, thinner Arctic ice cover: Increased potential for rapid, extensive sea-ice loss, *Geophys. Res. Lett.*, *34*, L24501, doi:10.1029/2007GL032043.

Meehl, G. A., C. Covey, T. Delworth, M. Latif, B. McAvaney, J. F. B. Mitchell, R. J. Stouffer, and K. E. Taylor (2007), The WCRP CMIP3 multi-model dataset: A new era in climate change research, *Bull. Am. Meteorol. Soc.*, *88*, 1383–1394, doi:10.1175/BAMS-88-9-1383.

Melling, H., and D. A. Riedel (2008), Ice Draft and Ice Velocity Data in the Beaufort Sea, 1990–2003, http://nsidc.org/data/g02177.html, Natl. Snow and Ice Data Cent., Boulder, Colo.

Merryfield, J. W., M. M. Holland, and A. H. Monahan (2009), Multiple equilibria and abrupt transitions in Arctic summer sea ice extent, in *Arctic Sea Ice Decline: Observations, Projections, Mechanisms, and Implications*, *Geophys. Monogr. Ser.*, vol. 180, edited by E. DeWeaver, C. M. Bitz, and B. Tremblay, 350 pp., AGU, Washington, D. C.

Parkinson, C. L., and W. M. Washington (1979), A large-scale numerical model of sea ice, *J. Geophys. Res.*, *84*(C1), 311–337, doi:10.1029/JC084iC01p00311.

Press, W. H., S. A. Tuekolsky, W. T. Vetterling, and B. P. Flannery (1992), *Numerical Recipes in FORTRAN*, 2nd ed., Cambridge Univ. Press, Cambridge, U. K.

Reynolds, R. W., and D. C. Marsico (1993), An improved real-time global sea-surface temperature analysis, *J. Clim.*, *6*(1), 114–119, doi:10.1175/1520-0442(1993)006<0114:AIRTGS>2.0.CO;2.

Reynolds, R. W., T. M. Smith, C. Liu, D. B. Chelton, K. S. Casey, and M. G. Schlax (2007), Daily high-resolution-blended analyses for sea surface temperature, *J. Clim.*, *20*(22), 5473–5496, doi:10.1175/2007JCLI1824.1.

Rothrock, D. A. (1975), Energetics of plastic-deformation of pack ice by ridging, *J. Geophys. Res.*, *80*(33), 4514–4519, doi:10.1029/JC080i033p04514.

Rothrock, D. A., and M. Wensnahan (2007), The accuracy of sea ice drafts measured from US Navy submarines, *J. Atmos. Oceanic Technol.*, *24*(11), 1936–1949, doi:10.1175/JTECH2097.1.

Rothrock, D. A., Y. Yu, and G. A. Maykut (1999), Thinning of the Arctic sea-ice cover, *Geophys. Res. Lett.*, *26*(23), 3469–3472, doi:10.1029/1999GL010863.

Rothrock, D. A., D. B. Percival, and M. Wensnahan (2008), The decline in arctic sea-ice thickness: Separating the spatial, annual, and interannual variability in a quarter century of submarine data, *J. Geophys. Res.*, *113*, C05003, doi:10.1029/2007JC004252.

Sanderson, B. M., C. Piani, W. J. Ingram, D. A. Stone, and M. R. Allen (2008), Towards constraining climate sensitivity by linear analysis of feedback patterns in thousands of perturbed-physics GCM simulations, *Clim. Dyn.*, *30*(2–3), 175–190, doi:10.1007/s00382-007-0280-7.

Steele, M., J. L. Zhang, D. Rothrock, and H. Stern (1997), The force balance of sea ice in a numerical model of the Arctic Ocean, *J. Geophys. Res.*, *102*(C9), 21,061–21,079, doi:10.1029/97JC01454.

Stroeve, J., M. M. Holland, W. Meier, T. Scambos, and M. Serreze (2007), Arctic sea ice decline: Faster than forecast, *Geophys. Res. Lett.*, *34*, L09501, doi:10.1029/2007GL029703.

Thorndike, A. S., D. A. Rothrock, G. A. Maykut, and R. Colony (1975), Thickness distribution of sea ice, *J. Geophys. Res.*, *80*(33), 4501–4513, doi:10.1029/JC080i033p04501.

Tucker, W. B., J. W. Weatherly, D. T. Eppler, L. D. Farmer, and D. L. Bentley (2001), Evidence for rapid thinning of sea ice in the western Arctic Ocean at the end of the 1980s, *Geophys. Res. Lett.*, *28*(14), 2851–2854, doi:10.1029/2001GL012967.

Vinje, T., N. Nordlund, and A. Kvambekk (1998), Monitoring ice thickness in Fram Strait, *J. Geophys. Res.*, *103*(C5), 10,437–10,449, doi:10.1029/97JC03360.

Vinnikov, K. Y., A. Robock, R. J. Stouffer, J. E. Walsh, C. L. Parkinson, D. J. Cavalieri, J. F. B. Mitchell, D. Garrett, and V. F. Zakharov (1999), Global warming and Northern Hemisphere sea ice extent, *Science*, *286*(5446), 1934–1937, doi:10.1126/science.286.5446.1934.

Wang, M. Y., and J. E. Overland (2009), A sea ice free summer Arctic within 30 years?, *Geophys. Res. Lett.*, *36*, L07502, doi:10.1029/2009GL037820.

Wensnahan, M., and D. A. Rothrock (2005), Sea-ice draft from submarine-based sonar: Establishing a consistent record from analog and digitally recorded data, *Geophys. Res. Lett.*, *32*, L11502, doi:10.1029/2005GL022507.

Williams, M. J., M. Bureau, and M. Cappellari (2010), The Tully Fisher relations of early type spiral and S0 galaxies, *Mon. Not. R. Astron. Soc.*, *409*(4), 1330–1346, doi:10.1111/j.1365-2966.2010.17406.x.

Witte, H., and E. Fahrbach (2005), AWI Moored ULS Data, Greenland Sea and Fram Strait, 1991–2002, http://nsidc.org/data/g02139.html, Natl. Snow and Ice Data Cent., Boulder, Colo.

Zhang, J., and W. D. Hibler (1997), On an efficient numerical method for modeling sea ice dynamics, *J. Geophys. Res.*, *102*(C4), 8691–8702, doi:10.1029/96JC03744.

Zhang, J., and D. A. Rothrock (2003), Modeling global sea ice with a thickness and enthalpy distribution model in generalized curvilinear coordinates, *Mon. Weather Rev.*, *131*(5), 845–861, doi:10.1175/1520-0493(2003)131<0845:MGSIWA>2.0.CO;2.

Zhang, J., and D. A. Rothrock (2005), Effect of sea ice rheology in numerical investigations of climate, *J. Geophys. Res.*, *110*, C08014, doi:10.1029/2004JC002599.

Zhang, J., M. Steele, and A. Schweiger (2010), Arctic sea ice response to atmospheric forcings with varying levels of anthropogenic warming and climate variability, *Geophys. Res. Lett.*, *37*, L20505, doi:10.1029/2010GL044988.

Zwally, H. J., D. H. Yi, R. Kwok, and Y. H. Zhao (2008), ICESat measurements of sea ice freeboard and estimates of sea ice thickness in the Weddell Sea, *J. Geophys. Res.*, *113*, C02S15, doi:10.1029/2007JC004284.

R. Kwok, Jet Propulsion Laboratory, California Institute of Technology, Mail Stop 300-331, 4800 Oak Grove Dr., Pasadena, CA 91109, USA.

R. Lindsay, A. Schweiger, M. Steele, H. Stern, and J. Zhang, Polar Science Center, Applied Physics Laboratory, University of Washington, 1013 NE 40th St., Seattle, WA 98105, USA. (axel@apl.washington.edu)